

Managing the Effects of Heat, Dust, and Vibration on a GPS Receiver in a Desert Environment

by

Stephen D. Thornton

A thesis submitted to the Graduate Faculty of
Auburn University
in partial fulfillment of the
requirements for the Degree of
Master of Science in Mechanical Engineering

Auburn, Alabama

May 7, 2016

Keywords: electronic packaging, solar radiation, GPS, desert environment, MATLAB,
SolidWorks

Copyright 2016 by Stephen D. Thornton

Approved by

George Flowers, Professor of Mechanical Engineering
and Dean of the Graduate School

David Bevly, McNair Endowed Professor of Mechanical Engineering

Jeffrey Suhling, Quina Distinguished Professor and Chair of Mechanical Engineering

Abstract

Applications for personal handheld electronic devices, such as GPS receivers, have significantly increased in recent years. It is now necessary for such devices to be able to operate in a wide variety of harsh environmental conditions. A desert environment poses several threats to electronic devices, such as heat, vibration, and dust. This creates a complex design challenge as techniques to reduce the effects of one condition can make the box more susceptible to another. This thesis details the tests performed and resulting design choices for ensuring that a GPS receiver would be able to operate in the midst of these harsh conditions. It was shown that solar radiation posed the greatest threat to the life and performance of the GPS receiver box. The threat of dust from the environment and the desire to decrease power consumption eliminated many commonly used active cooling techniques to control the interior temperature of the GPS receiver box. Instead, the effectiveness of several passive cooling methods, such as reflective tape, insulating coating, and a hood design was tested and the results have been detailed. A hood design was shown to be effective in protecting the GPS receiver box from solar radiation, but it was also shown that this design may not be necessary for a larger box. Vibration testing showed that using hex nuts with tooth washers held components more securely than regular hex nuts. The final individual components used to counteract the harsh environmental effects have also been discussed.

Acknowledgements

I would like to thank my advisor Dr. George T. Flowers for guidance and encouragement throughout this project. I would also like to thank Dr. David Bevly and Dr. Jeffrey Suhling for their evaluation and advice during this project. I would like to give a special thanks to Dr. William Travis, Ryan Hill, and Tony Simpson of Integrated Solutions for Systems, Inc. for their invaluable assistance and guidance during this project. I would also like to thank all my professors at Auburn University and the rest of the Auburn family for their incredible instruction, support, and encouragement throughout my time here. Finally, I would like to thank my parents and family for all the love and support they have given me throughout my life.

Table of Contents

Abstract	ii
Acknowledgements	iii
List of Figures	vii
List of Tables.....	x
Chapter 1 – Introduction and Literature Review.....	1
1.1 Problem Statement and Objectives	1
1.2 Common Solutions.....	3
1.3 Organization of Thesis	5
Chapter 2 – Thermal Testing	6
2.1 SolidWorks Simulation	6
2.2 Test Setup.....	8
2.3 Test Configuration Validation.....	9
2.3.1 The Numerical Model	9
2.3.2 Lab testing.....	12
2.3.3 Desert Testing and the Wind Model	18
2.4 Methods for Reducing Heating from Solar Radiation	23
2.4.1 Insulating Coating	25
2.4.2 Reflective Tape	27
2.4.4 Air Pocket	27
2.5 Hood Design	29
2.6 Desert Testing	31
2.6.1 Hood vs. No Hood	32

2.6.2 Powder Coating Test	34
2.6.3 Takachi vs. Hammond Box Comparison	36
2.6.4 Performance Tests	37
Chapter 3 – Vibration Testing.....	40
3.1 Test Setup.....	40
3.2 Test Results	42
Chapter 4 – Packaging Solution.....	44
4.1 Packaging	44
4.2 Circuit Board.....	45
4.3 Connectors	46
4.4 Battery	51
4.5 Mounting System	53
Chapter 5 – Summary and Conclusions.....	55
5.1 Summary and Conclusions.....	55
5.2 Future Work	55
5.2.1 Lab Testing.....	55
5.2.2 Desert Testing	56
References	57
Appendix A	59
CalculatePowerValues.m	59
SimulatePlate.m	63
YumaTripPlateAnalysis.m.....	69
MethodComparison.m.....	74
Appendix B	80

Air Property Tables 80

List of Figures

Figure 2-1 SolidWorks Simulation with No Solar Load.....	6
Figure 2-2 SolidWorks Simulation with Solar Loading on the Top Surface.....	7
Figure 2-3 SolidWorks Simulation with Solar Loading on the Front Surface.....	7
Figure 2-4 Full Radiation Test Setup.....	9
Figure 2-5 Plate with Thermocouple Beneath the IR Lights	13
Figure 2-6 Calculated Heat Input from IR Lights at Height 1	14
Figure 2-7 Calculated Heat Input from IR Lights at Height 2	15
Figure 2-8 Calculated Heat Input from IR Lights at Height 3	15
Figure 2-9 Simulation of the Plate at Height 1	16
Figure 2-10 Simulation of the Plate at Height 2	17
Figure 2-11 Simulation of the Plate at Height 3	17
Figure 2-12 Solar Loading During the Course of a Day.....	18
Figure 2-13 Yuma Plate Test Simulation.....	20
Figure 2-14 Test Setup with Wind.....	21
Figure 2-15 Wind Simulation of the Plate at Height 1	21
Figure 2-16 Wind Simulation of the Plate at Height #2	22
Figure 2-17 Wind Simulation of the Plate at Height #3	22
Figure 2-18 Blank Box with No Coating.....	24
Figure 2-19 Thermal Imaging of Heat Test	25
Figure 2-20 Empty Box with Internal Coating	26
Figure 2-21 Coating vs. No Coating Comparison.....	26
Figure 2-22 Reflective Tape vs. No Coating Comparison.....	27
Figure 2-23 Test Setup for Air Pocket Test	28

Figure 2-24 Air Pocket vs. No Coating Comparison	29
Figure 2-25 Hood Design.....	30
Figure 2-26 Hood Test Setup	30
Figure 2-27 Hood Test Results	31
Figure 2-28 Hood vs. No Hood Test.....	32
Figure 2-29 Hood vs. No Hood Results Day 1	33
Figure 2-30 Hood vs. No Hood Results Day 2	33
Figure 2-31 Powder Coating Static Test	35
Figure 2-32 Powder Coating Dynamic Test	36
Figure 2-33 Takachi vs. Hammond Box Comparison	37
Figure 2-34 Hitachi Box on a Military Vehicle	38
Figure 2-35 Hammond Box with Hood on the SUV.....	39
Figure 3-1 Composite Wheeled Vehicle Vibration Exposure.....	40
Figure 3-2 Vibration Testing in the Vertical Direction.....	41
Figure 3-3 Vibration Testing in the Transverse Direction	41
Figure 3-4 Vibration Testing in the Longitudinal Direction	42
Figure 3-5 New Nut used for the GPS Receiver	43
Figure 3-6 The Clamping Nut Holding the GPS Receiver	43
Figure 4-1 Enclosure with Silicon Protector	44
Figure 4-2 Circuit Board in the Box	45
Figure 4-3 Components on the Board	46
Figure 4-4 LED Lights and Computer Board Connection	47
Figure 4-5 Screen and Power Latching Connections	47
Figure 4-6 Latching Connection for Screen Backlight	48

Figure 4-7 Latching Connection for Push Buttons 48

Figure 4-8 Interior Side Wall with Connection Ports for Exterior Components 49

Figure 4-9 Exterior Connection Ports 50

Figure 4-10 Connection from GPS Receiver to Antenna 51

Figure 4-11 Battery Box with Internal Foam..... 52

Figure 4-12 Battery Box Before Mounting to the Receiver Box 52

Figure 4-13 Battery Box Mounted to the Receiver Box 53

Figure 4-14 Mounting System 54

List of Tables

Table 2-1 Heights Used for Tests.....	13
Table 2-2 Power Inputs at Different Heights	16
Table 2-3 Wind Speeds	20

Chapter 1 – Introduction and Literature Review

As the use of electronic devices continues to expand, a great deal of research is currently being done to allow electronics to operate under a variety of harsh conditions. Not only are electronic devices being used in harsher conditions, but they are also performing more functions than ever before. As the processing capabilities of electronics increases, so does the need to dissipate heat generated by the operation of these devices. This can be particularly difficult in hotter environments. This literature describes the process of developing and testing a GPS receiver box capable of computing position data while withstanding the harsh environmental factors associated with a desert environment.

1.1 Problem Statement and Objectives

The goal of this project is to design a GPS receiver box capable of maintaining a high level of performance in the harshness of a desert environment. The operator using this receiver box will be driving a tracked military vehicle in a convoy in the desert. A series of LED lights are used as a warning system to alert drivers if they approach a vehicle too quickly, while a screen also reports the distance to the next vehicle. A desert environment poses many threats to electronic equipment, such as extreme heat, dust, and vibrations. Many common solutions to counter some of these effects would make the device more susceptible to other effects. This makes it a challenge to balance different design goals.

The primary goal for this project was for the GPS receiver box to maintain performance goals despite environmental conditions. Among environmental factors that influence reliability, temperature does the most to accelerate the degradation of electronic components [1] [2]. High temperatures can cause electronic components to degrade chemically and fail catastrophically [1]. Low temperatures and thermal shock can also cause mechanical stress within structural elements, as a result of different materials having different coefficients of thermal expansion [3]. However, for this application, high temperatures pose the most threat to electronic components in the receiver box. In particular, solar radiation in desert regions can be detrimental to electronics. Aluminum aircraft parked in these conditions can reach internal

temperatures of 74° C [2]. This created a challenge, since the internal components used for the GPS receiver box were specified to operate below 60° C. Keeping the internal temperature of the box below this critical temperature was one of the primary goals of this project.

Dust and sand could also reduce the performance and lifetime of the GPS receiver box. Electronic components which are most harshly affected by dust and sand are devices that involve moving parts, or photovoltaic cells [3] [4]. Dust and sand reduce the lifetime of electronic components because they are abrasive, which increases the wear on components. They also create friction which increases the production of heat and causes mechanical wear. Finally, they can clog openings and prevent air or light from moving through [3]. All of these factors limit cooling techniques which can be used to lower the internal temperature of the GPS receiver box. However, even in a system with no moving parts or photovoltaic cells, dust can still negatively affect a circuit board. A buildup of dust or sand can insulate a component, making it more susceptible to overheating [5]. Under normal circumstances, sand and dust do not conduct electricity [6]. However, if dust contains any conductive materials, such as water, oils or metallic elements, it can cause electrical contact between two components and create a short circuit [5]. Overall, the GPS receiver will be able to perform most efficiently if the box is sealed effectively against dust and sand.

The final environmental factor threatening the performance and lifetime of the GPS receiver box is vibrations. The GPS receiver box is intended to be used for a military application on a tracked vehicle in the desert. The vehicle itself, along with uneven terrain over which it travels, creates significant vibrations to which the GPS receiver box will be exposed. Exposure to vibrations can cause screws and other clamping devices to loosen and can mechanically damage components such as circuit boards [7]. These effects can be immediate, or long term exposure can cause components to fatigue and fail before they normally would do so. Both immediate and long term effects of vibration can prove to be catastrophic, and therefore the box must be designed specifically to withstand these conditions.

Along with the basic functional performance goals for the GPS receiver box, there are several other goals for this project. Keeping the box as small as possible ensures that its users could

easily transport and mount it. The box also needs to have its own power supply, while remaining easily portable. This makes it very desirable for the box to have as low power consumption as possible. However, there are limits to how low the power supply can be, since the screen and LED lights need to be easily readable in the direct sunlight of the desert. The final objective is for the box to be composed of generic components that can easily be swapped out in the event of a failure. Not using custom parts saves money on the design, but makes it harder to maximize spatial efficiency.

1.2 Common Solutions

Many current solutions exist to reduce the effects of the conditions previously mentioned. One of the most common electronic cooling solutions is air cooling with a fan. This process typically pulls ambient air into the enclosure to cool components [8]. Air cooling faces several significant challenges in a desert environment. A fan would increase the power supply needed to operate the system, and require a complex filtration system to prevent dust from clogging the fan. This filtration system would need to be cleaned regularly, to avoid losing efficiency. The amount of dust in a desert environment would make this cooling strategy difficult to implement.

Liquid cooling is another common cooling technique for electronics, which can be more effective than air cooling [9]. This is typically done by bringing the liquid into contact with a conducting plate attached to the electronic components, or sometimes bringing the coolant into direct contact with the electronic component [9]. This method could be effective for the GPS receiver box, but it would drastically increase the cost to manufacture the box. Also, the water lines would need to be able to withstand the vibrations the box would encounter, since a leak would prove to be catastrophic. The biggest deterrent for using a liquid cooled system in the GPS receiver box is the limited power supply. Pumping the liquid through the system would drastically increase the power supply needed to power the box. It would also increase the cost to manufacture the box.

As a result of the limited power supply, the most desirable methods for reducing the internal temperature of the GPS receiver box involve cooling without a power supply, or passive

cooling. Passive cooling can be created in multiple ways. Using highly conductive walls for the box enclosure allows heat to dissipate from the inside of the box to the environment, when the internal temperature exceeds the ambient temperature [8]. Providing shade on the external surface of the enclosure can minimize the heating effects from solar radiation [8]. Solar radiation can also be limited through the selection of the external surface color or material. Selecting a material or color with a high reflectivity will limit the amount of solar energy absorbed by the box [10]. Passive cooling can also be done by increasing the heat capacitance of the overall box. Having a larger box will require a greater amount of heat to raise the internal temperature. This causes the temperature within the box to fluctuate less than the temperature of the environment around the box [8]. This is advantageous, since the box will experience the greatest heat load in the middle of the day and little to no heat load during the night. However, the need for the box to remain easily portable limits the size of the box that can be used. Overall, passive cooling techniques seem the most advantageous for the GPS receiver box as a result of their simplicity and low cost to both implement and operate [8]. The main drawback is that these techniques are limited in their cooling capabilities. However, if passive cooling techniques can be implemented so as to maintain the box below the critical temperature of 60° C, they are highly preferable over more complicated and expensive active cooling methods.

While there are multiple techniques to reduce the effects of high temperatures, the main solution to reduce the impact of dust is simply to enclose the system. Designing the box so that internal components are sealed from the external environment is the only way to fully prevent dust from effecting the performance of the internal components. Likewise, there are only two strategies to reduce the impact of vibrations on the electronics components. The box can either be isolated from the vibrations, or the components can be designed to withstand the effects of vibrations [3]. The first method is used when selecting a way to mount the receiver box. The second method is used when selecting connectors and mounting techniques used within the receiver box.

1.3 Organization of Thesis

This work details the design choices and tests that were performed to ensure that the GPS receiver box would achieve its required level of performance under the conditions previously described. Chapter 2 discusses the thermal testing that was conducted. This includes initial CAD tests, the development of test rig used in the lab, and tests performed in the actual desert environment. Chapter 2 also discusses various methods that were used to minimize the impact of solar loading on the box. Chapter 3 discusses vibration testing that was performed on the box. Chapter 4 discusses the box design, and reasons behind the selection of individual components. Chapter 5 summarizes the results and conclusions of this project and discusses the work that still need to be done in order to ensure that the GPS receiver box maintains the proper level of performance once it is implemented.

Chapter 2 – Thermal Testing

One of the biggest challenges facing the use of electronic devices in a desert environment is the extreme heat. Overheating can cause components to malfunction within the receiver box. Cooling fans are traditionally used to lower the internal temperature of electronics. However, electronics in a desert environment must be completely sealed because the sand and dust would otherwise get inside and cause the device to fail. While the high ambient temperature is a concern, the primary concern is the high input of solar radiation in this region.

2.1 SolidWorks Simulation

To obtain an approximated understanding of how the box would heat up, a model was created in SolidWorks. The first simulation, shown in Figure 2-1, used an ambient temperature of 48.9° C. In this simulation, heat was generated from the internal components, with no solar loading.

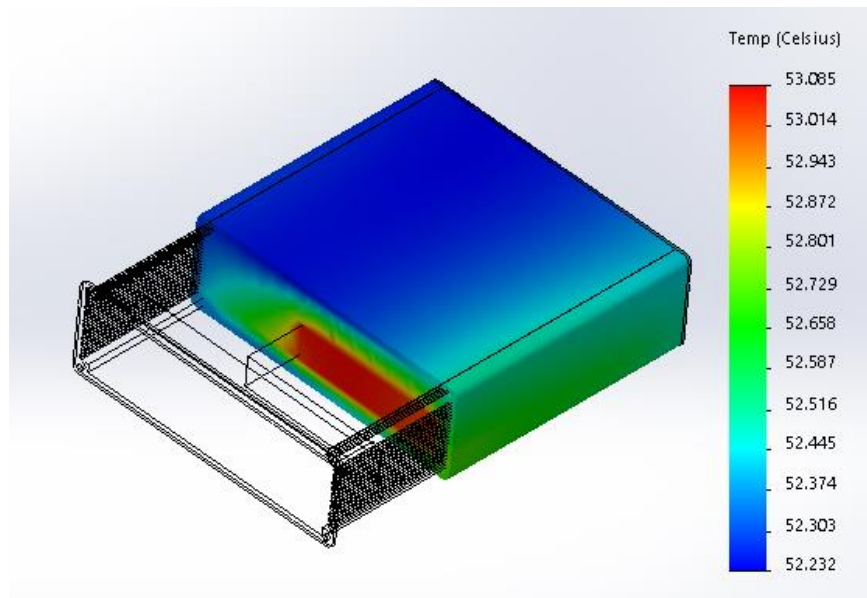


Figure 2-1 SolidWorks Simulation with No Solar Load

With no solar loading, the box stayed under the critical temperature of 60° C, reaching a maximum temperature of 53.1° C. Two more simulations were performed with a solar load of

1120 W/m² placed directly onto the front and top surface of the box, to simulate a worst case scenario. The results are shown in Figures 2-2 and 2-3.

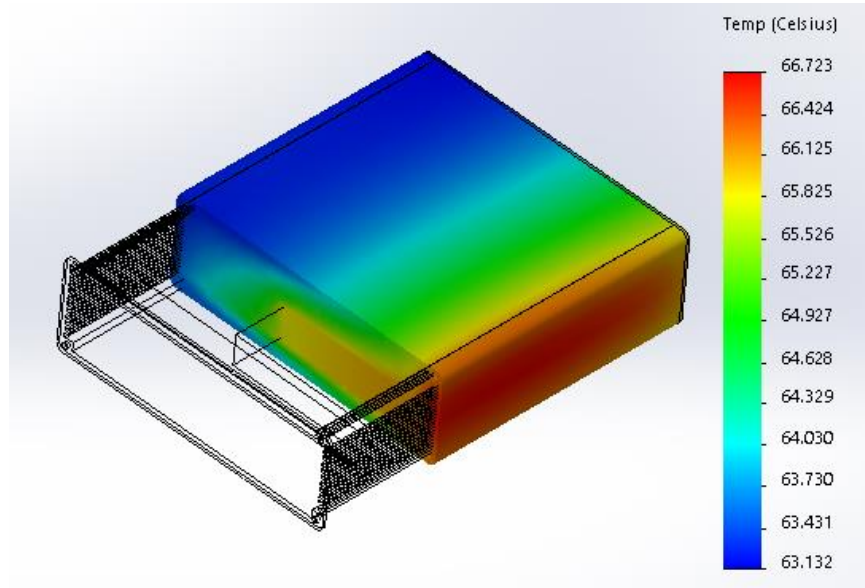


Figure 2-2 SolidWorks Simulation with Solar Loading on the Top Surface

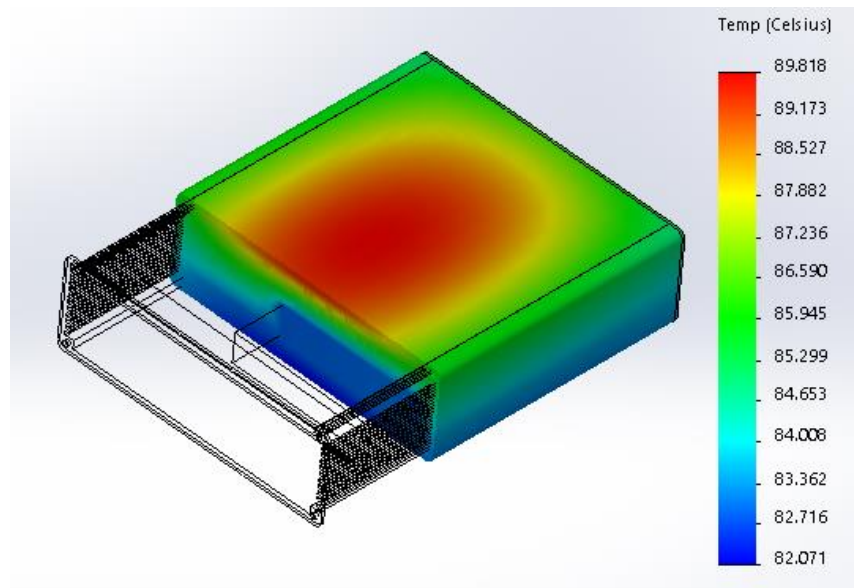


Figure 2-3 SolidWorks Simulation with Solar Loading on the Front Surface

In both cases for which the solar load was included, the box exceeded the critical temperature. The box reached 66.7° C and 89.8° C when the solar load was placed on the top and front surfaces, respectively. This shows that solar heating is a far greater threat than heating from the internal electronic components.

2.2 Test Setup

According to MIL-STD-810G, solar radiation in hot dry climates, such as Yuma, can reach 1120 W/m² [11]. In order to test various methods to minimize the effects of solar radiation, it was necessary to develop a reliable way to create a radiated heat load similar to the effects of solar radiation. While it seems reasonable to perform these tests outside in direct sunlight, varying wind and cloud cover could make the results inconclusive. Two 250-watt infrared light bulbs were used instead. They were placed next to each other in a lighting fixture, which was then mounted to an aluminum 80/20 frame. The 80/20 frame allowed for the lights to be moved up and down, which would increase or decrease the radiative heat input on the item being tested. The whole device is shown in Figure 2-4.



Figure 2-4 Full Radiation Test Setup

2.3 Test Configuration Validation

In order to estimate the heat load that the bulbs would give off during a test, a steel plate with known properties was tested and compared to a mathematical model. A 1018 cold rolled low carbon steel plate was used. This plate was 15.24 cm by 20.32 cm. and .3175 cm thick. It was estimated that the specific heat of the plate was 486 J/kg and the emissivity was .8 [12].

2.3.1 The Numerical Model

The heat transfer of the plate was assumed to behave according to Equation 2.1

$$C_p \frac{dT_s}{dt} = Q_{rad} + Q_{conv} + Q_{light} \quad (2.1)$$

where

$$C_p = \text{Specific Heat in } \frac{J}{^\circ C}$$

$$\frac{dT_s}{dt} = \text{The change of temperature w.r.t time in } \frac{^\circ C}{s}$$

$$Q_{rad} = \text{Heat radiating from the plate to the environment in } W$$

$$Q_{conv} = \text{Heat leaving the plate due to convection in } W$$

$$Q_{light} = \text{Heat entering the plate from the IR light in } W$$

The heat entering the plate from the IR light was estimated using the following equation.

$$Q_{light} = G_s \alpha_s$$

where

$$G_s = \text{Irradiation hitting the plate in } W$$

$$\alpha_s = \text{Solar absorptivity}$$

The solar absorptivity, α_s , of cold rolled low carbon steels has been shown to be around .6 for wavelengths in the IR range, so that is what was used for the estimate [12] [13].

The heat radiating from the plate to the environment was estimated to behave according to Equation 2.2

$$Q_{rad} = \epsilon \sigma A (T_a^4 - T_s^4) \quad (2.2)$$

where

$$\epsilon = \text{emissivity}$$

$$\sigma = \text{Stefan Boltzmann Constant} = 5.670373 * 10^{-8} \frac{W}{m^2 K^4}$$

$A = \text{area of the top surface of the plate in } m^2$

$T_a = \text{ambient temperature in } K$

$T_s = \text{plate surface temperature in } K$

The emissivity, ϵ , of cold rolled steel is typically between .75 and .85. so a median value of .8 was used as a best estimate. The heat leaving the plate due to convection was modelled according to Equation 2.3

$$Q_{conv} = HA(T_a - T_s) \quad (2.3)$$

Equation 2.4 was used to find the convection coefficient, H .

$$H = k * \frac{Nu}{L} \quad (2.4)$$

The thermal conductivity of air, k , is a temperature dependent property that was solved for using interpolation each iteration. The effective length of the plate, L , was found using equation 2.5

$$L = \frac{A_s}{P} \quad (2.4)$$

where A_s and P are the surface area and perimeter of the top of the plate. The Nusselt Number, Nu , was found using Equation 2.5.

$$\overline{Nu}_L = 0.54Ra_L^{\frac{1}{4}} (10^4 \leq Ra_L \leq 10^7, Pr \geq 0.7) \quad (2.5)$$

The condition for the Prandtl number, Pr , remained throughout the simulations. The Raleigh number, Ra , did drop below this assumed condition when the temperature of the plate was very close to the ambient temperature. Since these simulations focus on the time when the plate was

much hotter than ambient temperature, this effect was negligible. The Raleigh number was found using Equation 2.6

$$Ra_L = \frac{g\beta(T_s - T_a)L^3}{\nu\alpha} \quad (2.6)$$

where

$$g = \textit{Gravitational acceleration} = 9.807 \frac{m}{s^2}$$

$$\beta = \textit{Thermal expansion coefficient} = \frac{1}{T_f}$$

T_f is the average of T_s and T_a . This is the temperature used to determine the thermal diffusivity of air, α , kinematic viscosity of air, ν , Prandtl number, and thermal conductivity of air. These properties were calculated using interpolation during each iteration of the simulation.

2.3.2 Lab testing

To test the IR light, a piece of cardboard was placed on top of some wooden pallets. The rig was then placed on top of the cardboard, and sand was used to fill the base of the rig. The steel plate was placed on an insulating sheet with k-type thermocouples mounted to the top surface of the plate, as shown in Figure 2-5. The insulating sheet, pallets, cardboard, and sand were used to prevent the cold concrete ground from acting as a heat sink to the plate. The reason sand was chosen was because this experiment would later be repeated on the ground in the desert, and this provided comparable results between the two tests. Three different heights were chosen for the test. These heights are shown in Table 2-1.



Figure 2-5 Plate with Thermocouple Beneath the IR Lights

Table 2-1 Heights Used for Tests

Height	Height (cm)
1	15.24
2	30.48
3	45.72

The thermocouples were attached to a data logger, which recorded the plate top surface temperature every 30 seconds, along with the ambient temperature. The light was then turned on at the three different heights above the plate. When the plate reached steady state, the light was turned off and the temperature data was recorded until the plate cooled down to ambient temperature.

The temperature data was then smoothed and differentiated to find the heat input by rearranging Equation 2.1 to the form

$$Q_{light} = C_p \frac{dT}{dt} - Q_{rad} - Q_{conv}$$

The value of Q_{light} was then calculated for each recorded temperature while the light was on. The results are shown in Figure 2-6, 2-7, and 2-8.

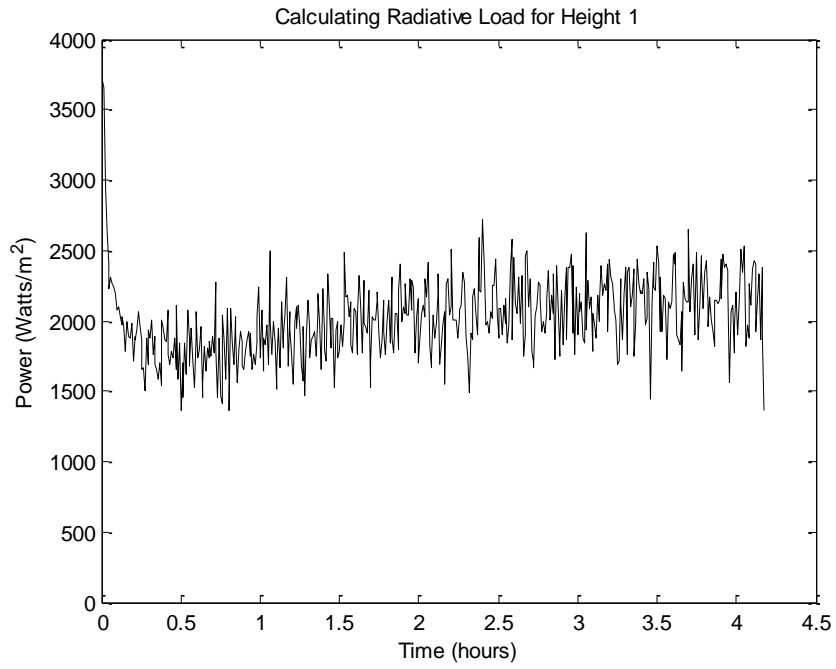


Figure 2-6 Calculated Heat Input from IR Lights at Height 1

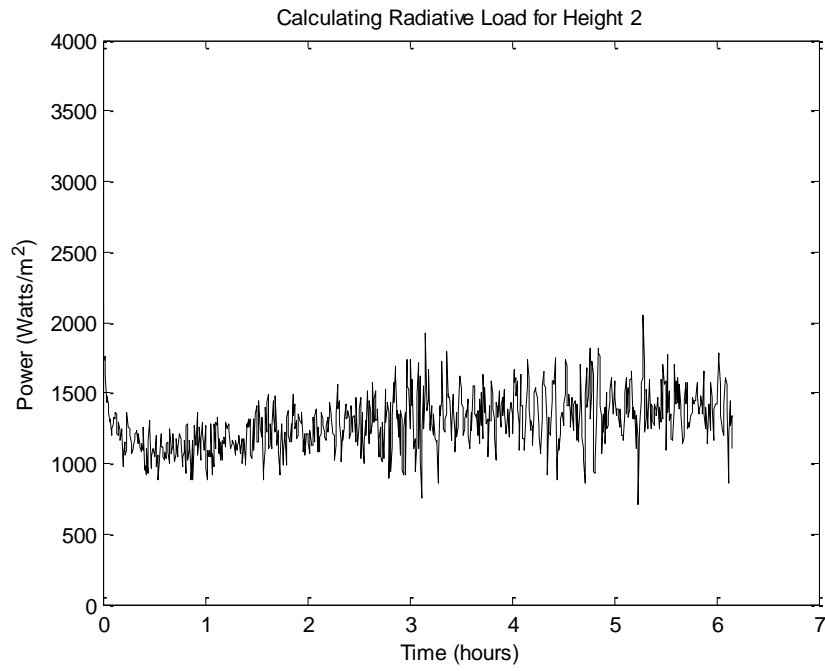


Figure 2-7 Calculated Heat Input from IR Lights at Height 2

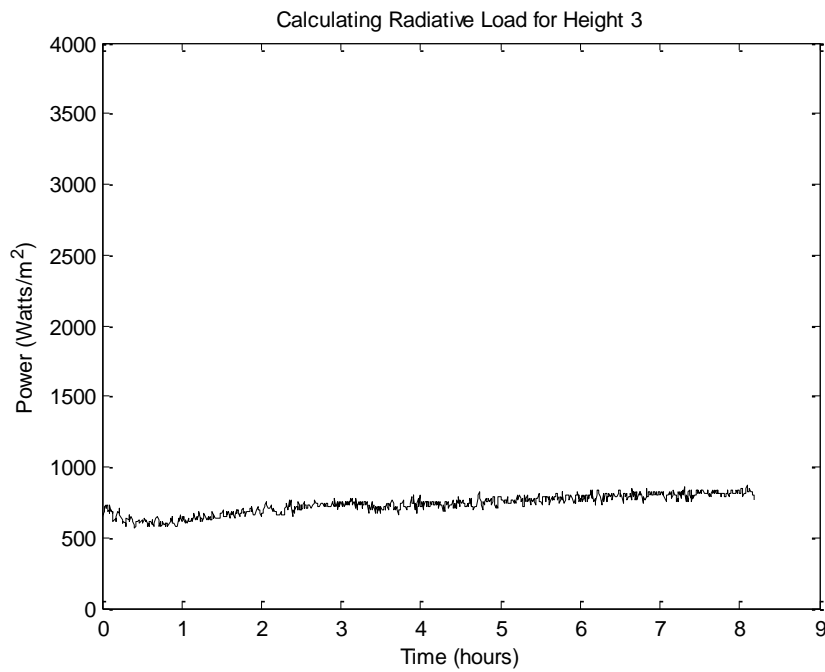


Figure 2-8 Calculated Heat Input from IR Lights at Height 3

The average of Q_{light} was then taken once it had stabilized at a steady state. These values, shown in Table 2-2, were then used to simulate the the temperature of the plate using T_a as an input. The results are shown in Figure 2-9, 2-10, and 2-11.

Table 2-2 Power Inputs at Different Heights

Height	Heat Input (W/m ²)
1	2,110.9
2	1,375.4
3	813.3

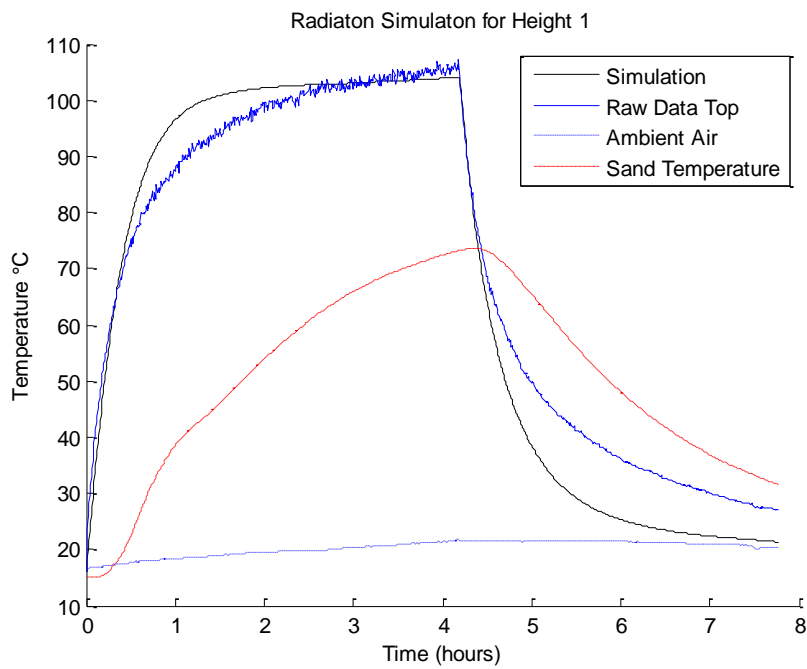


Figure 2-9 Simulation of the Plate at Height 1

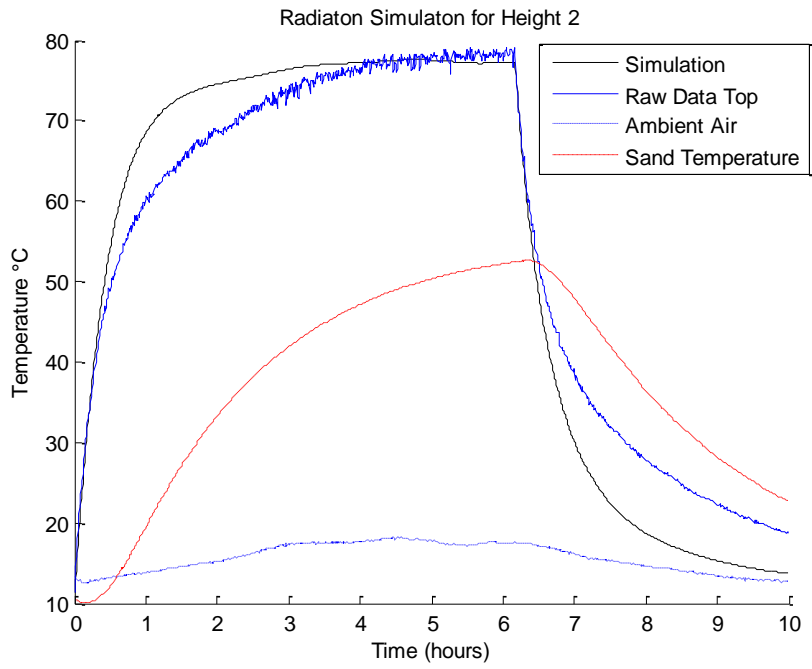


Figure 2-10 Simulation of the Plate at Height 2

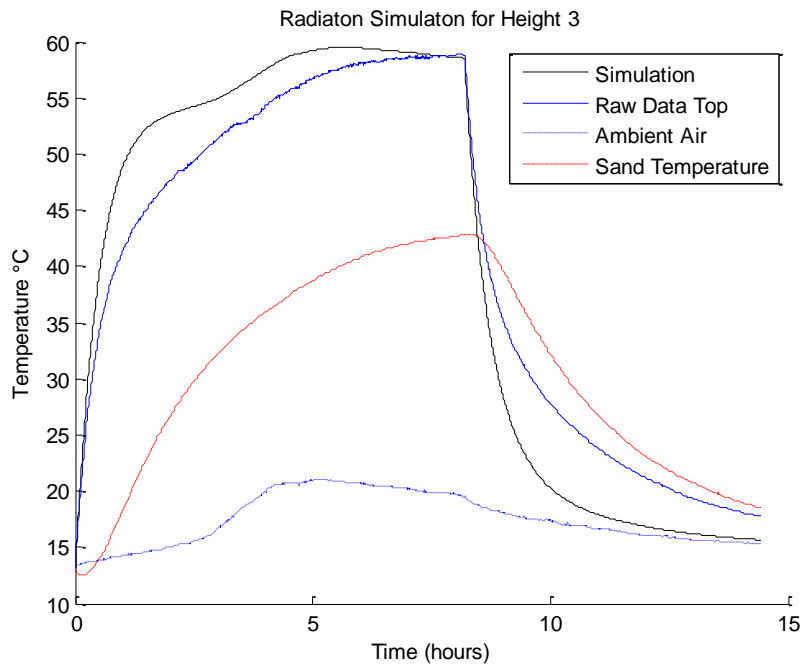


Figure 2-11 Simulation of the Plate at Height 3

The simulations correlate well with the raw data, so the irradiation from the light at Height 1, Height 2 and Height 3 was taken to be 2,1109 W/m², 1,375 W/m², and 813 W/m², respectively.

2.3.3 Desert Testing and the Wind Model

To verify the model, the plate was placed on the ground and left to heat during one of the hottest days in Yuma. The insulating sheet was placed between the plate and the desert sand, similarly to the test rig. The solar load was calculated in the same manner previously described. It was assumed that the solar load would change throughout the course of a day, so instead of averaging the solar load, a polynomial fit was applied. Karim and Singh showed that a 5th degree polynomial fit matches the solar radiation hitting the ground during the course of a day, so this type of fit was used [14]. The results are shown in Figure 2-12.

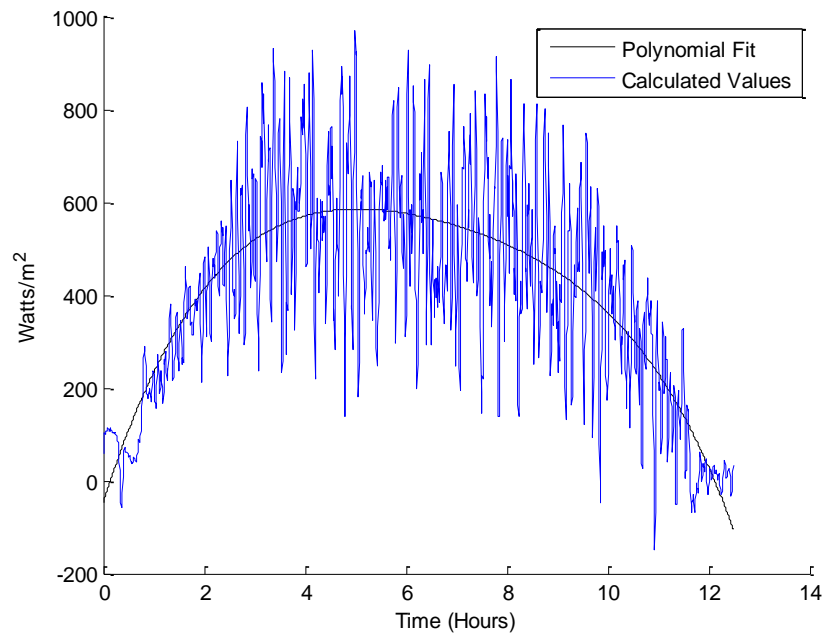


Figure 2-12 Solar Loading During the Course of a Day

Even though the temperature data was smoothed before being integrated to find the heat input, the resulting values still ended being very noisy, and fell short of the assumed maximum load

of 1120 W/m². The main difference between this test and the previous tests was that in previous tests the plate was assumed to cool due to natural convection. This assumption was acceptable in a controlled environment, since air moving across the plate was minimal. However, for the test in the desert, it was not possible to completely block wind without shading the plate at some point during the day. Weather services recorded the average wind speed during that day to be over 5 m/s and the maximum wind speed to be over 9 m/s [15]. These measurements are typically taken about 10 meters above the ground, so the wind speed at the plate would likely be lower [16]. Nevertheless, a new model needed to be used to account for the wind. Equations 2.1 to 2.4 still apply for forced convection. The Nusselt number was then found using the following equation

$$\overline{Nu}_L = 0.664Re_x^{\frac{1}{2}} Pr^{\frac{1}{3}}, \quad (Pr \geq 0.7) \quad (2.7)$$

where the Reynold's number, Re , was found

$$Re_x = \frac{VL}{\nu} \quad (2.7)$$

$$V = \text{wind velocity in } \frac{m}{s}$$

The polynomial fit for the solar load was then scaled so that the maximum amount of solar radiation was 1120 W/m². The wind speed was then found to be 0.3 m/s. These parameters were then simulated and compared to the raw data, as shown in Figure 2-13.

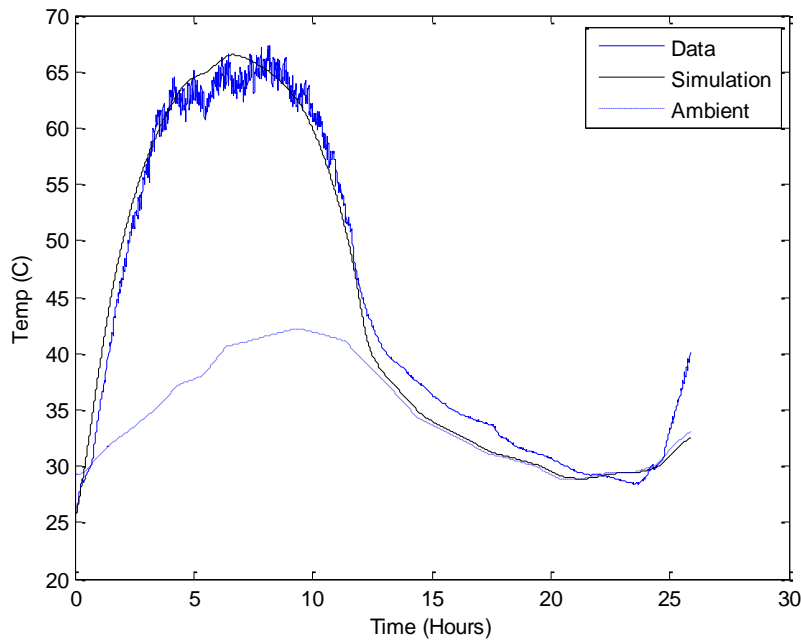


Figure 2-13 Yuma Plate Test Simulation

To verify the wind model, the tests under the IR heat lamp were repeated with a fan blowing air across the plate. A handheld wind speed indicator was used to measure the wind speed across the plate. The measured wind speeds are shown in Table 2-3. The test setup is shown in Figure 2-14. Tests were then run with the fan blowing at the three different heights. The results are shown in Figure 2-15, 2-16, and 2-17.

Table 2-3 Wind Speeds

Height	Wind Speed (m/s)
1	1.2
2	1.8
3	1.3

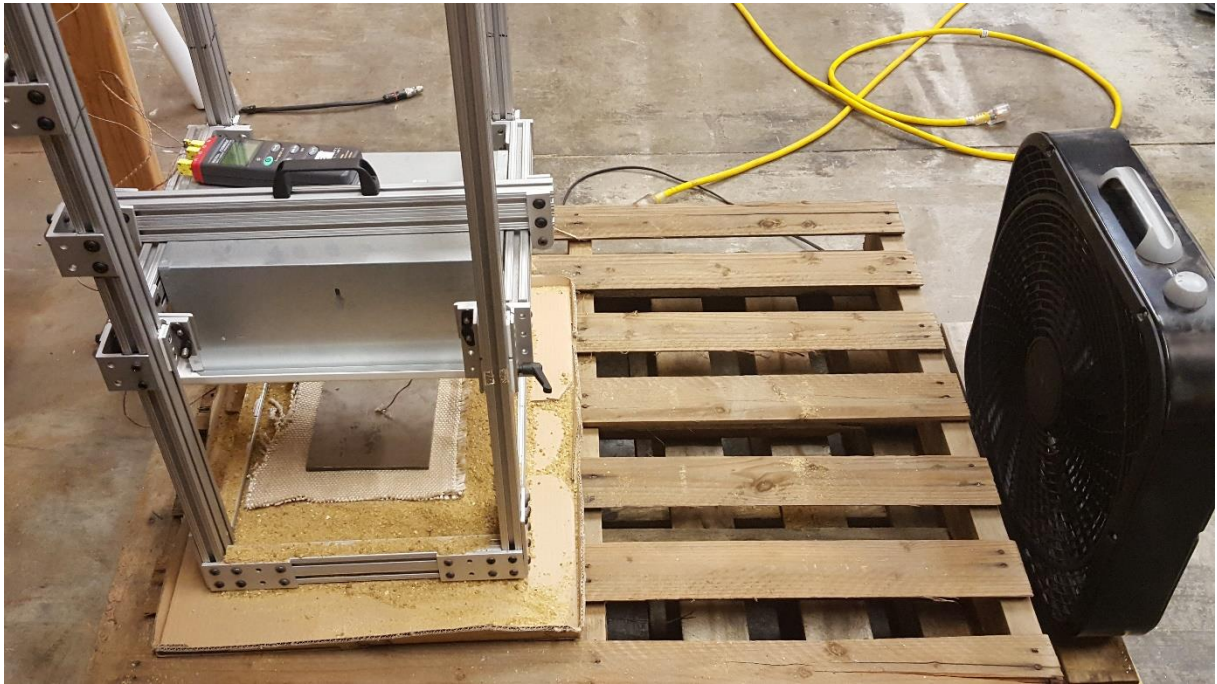


Figure 2-14 Test Setup with Wind

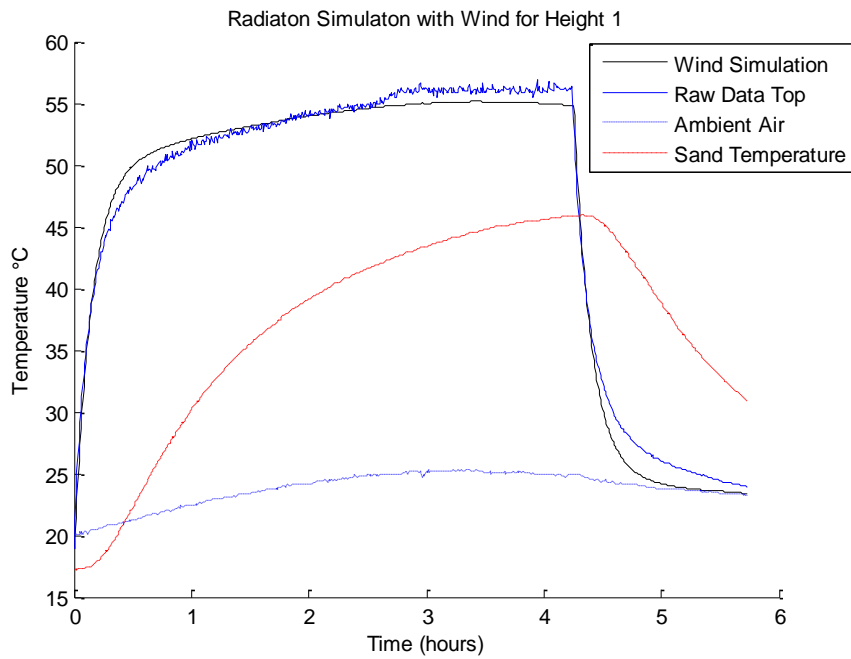


Figure 2-15 Wind Simulation of the Plate at Height 1

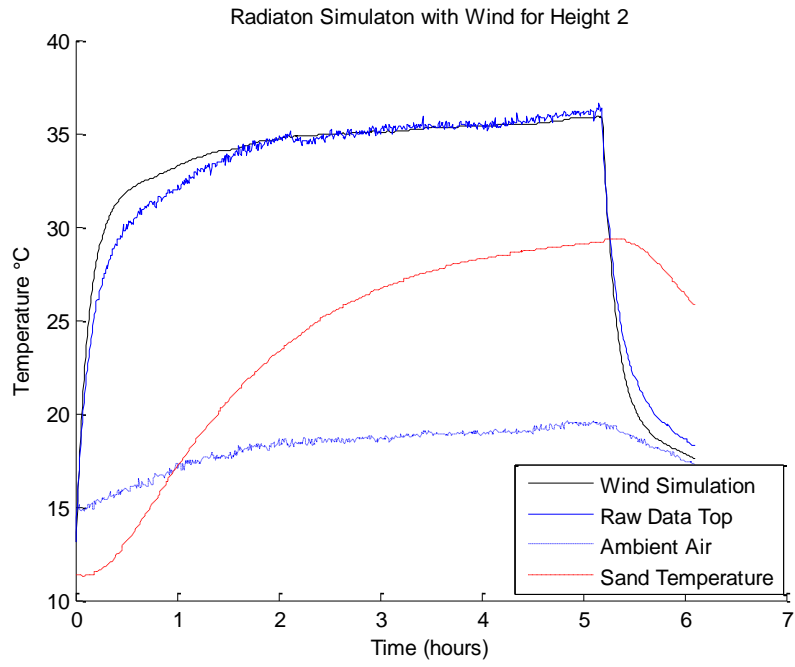


Figure 2-16 Wind Simulation of the Plate at Height #2

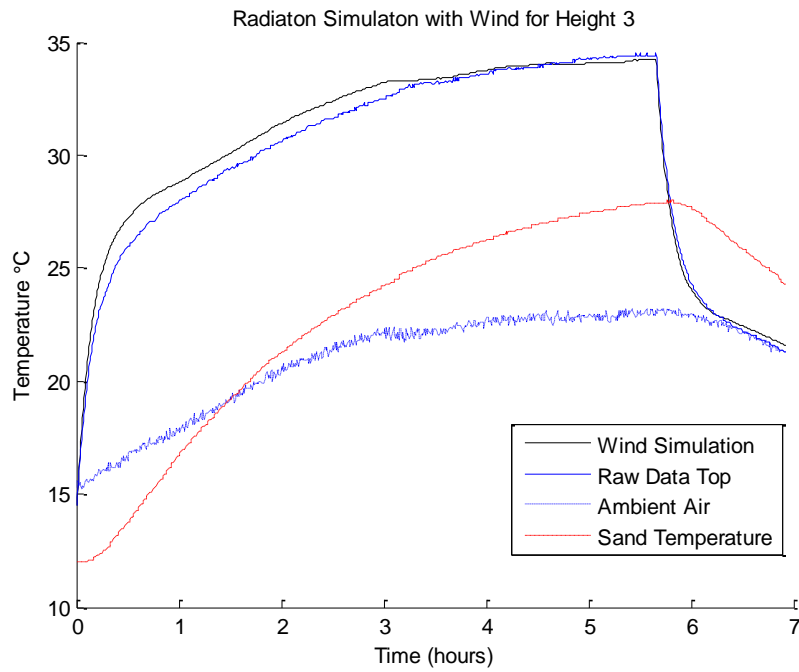


Figure 2-17 Wind Simulation of the Plate at Height #3

These simulations show that the numerical model that includes effects of wind correlates well with the results of the experimental test. This validates the model, and shows that a height between Height 2 and Height 3 can be used to simulate the actual solar radiation experienced in the desert.

2.4 Methods for Reducing Heating from Solar Radiation

Once the test setup was complete, it was possible to test different methods to reduce the internal temperature of the GPS receiver box. The primary goal is to design the box so that the interior temperature does not exceed 60° C. If the internal temperature of the box exceeds this critical temperature, the components within the box could fail. Another primary goal is for the box to be able to operate in the dust and vibrations expected in a desert environment. A secondary goal is to minimize power consumption. This makes it desirable to seek passive cooling methods rather than attempt to implement an air or water cooled system.

In order to obtain an initial baseline, the test setup was used to heat an empty box similar to the receiver box. A k-type thermocouple was attached to the inside of the box so that the exposed end was located in the center of the box, as shown in Figure 2-18.



Figure 2-18 Blank Box with No Coating

The box was then assembled and sealed, with the exception of the small screw hole through which the thermocouple went into the box. Another k-type thermocouple was then attached to the top surface of the box, and a third thermocouple was used to measure ambient temperature. Heat resistant reflective tape was used to attach the interior and exterior thermocouples. Thermal imaging showed that this tape did have an impact on the test by creating a cooler area on the surface of the box, as shown in Figure 2-19. As a result, extra care was taken to minimize the amount of tape used and to use the same amount of tape for each test.

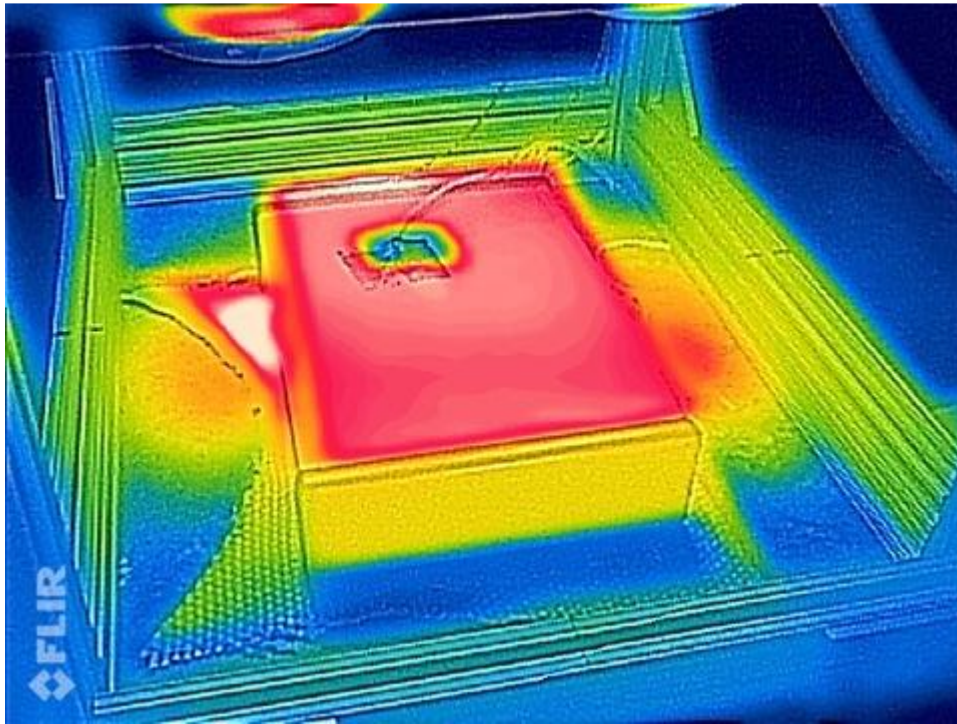


Figure 2-19 Thermal Imaging of Heat Test

2.4.1 Insulating Coating

One of the first methods examined for minimizing the effects of solar radiation was the use of an insulating coating. A ceramic thermal insulation coating was used, which is primarily used to insulate cars and reduce heating from solar radiation [17]. To test whether the insulation coating would work for the GPS receiver box, an empty box was coated as shown in Figure 2-20. The same test procedure was followed as previously described for the receiver box with no coating. Figure 2-21 compares the results of these two tests.



Figure 2-20 Empty Box with Internal Coating

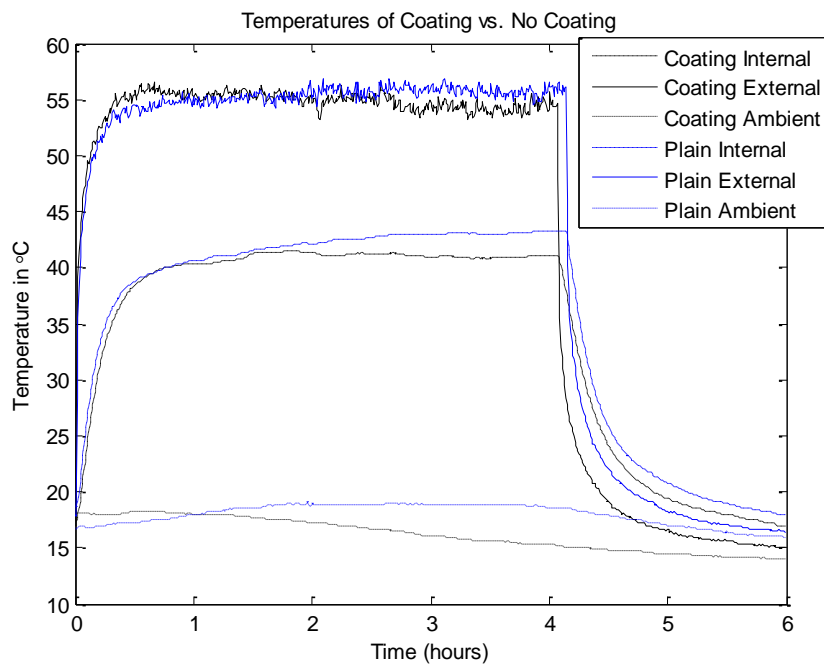


Figure 2-21 Coating vs. No Coating Comparison

From the tests, there appears to be a very small temperature difference between the box with the coating and the box without the coating. This temperature difference seems to be caused by the difference in ambient temperature during each test, rather than the effects of the coating. As a result, other passive cooling techniques were examined.

2.4.2 Reflective Tape

The next passive cooling method examined was to use the reflective, high temperature tape that was previously used to attach the thermocouples. The reflectivity of the tape would allow less solar radiation to be absorbed by the box, causing less internal heating. This tape was used to cover the exterior of the box, and the same test procedure described earlier was repeated. The results are shown in Figure 2-22.

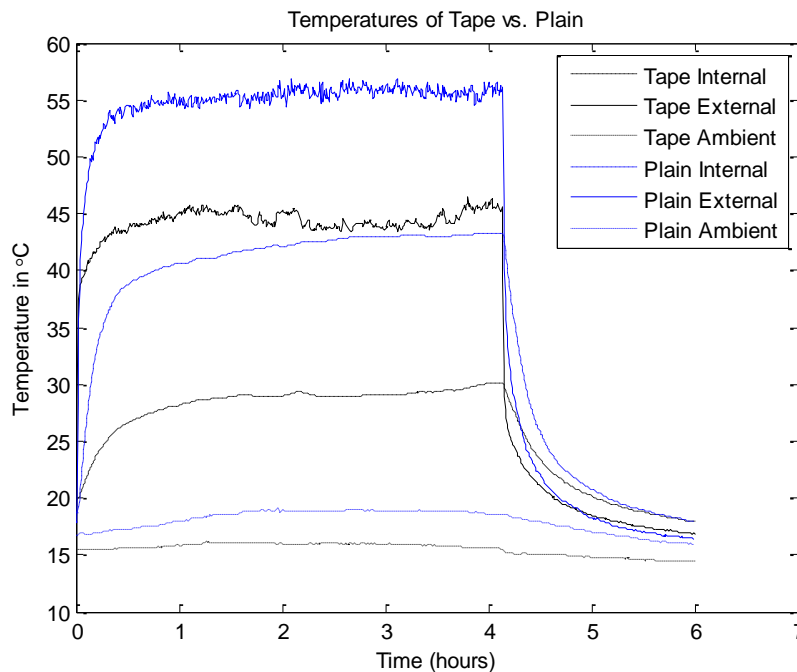


Figure 2-22 Reflective Tape vs. No Coating Comparison

The reflective tape performed much better than the insulative coating. However, it was not an ideal solution for the GPS receiver box, since the reflected light could potentially distract the driver looking at the receiver box. Other options were examined with the understanding that the tape could be utilized if a better alternative could not be found.

2.4.4 Air Pocket

The final passive cooling method considered was to create an air pocket surrounding the box.

To test this concept, a piece of sheet metal was bent so that it would surround the receiver box. An air pocket remained in between the box and the sheet metal as shown in Figure 2-23. Thermocouples were used to measure the temperature the exterior of the box, the air on the interior of the box, and ambient air. The results are shown in Figure 2-24.

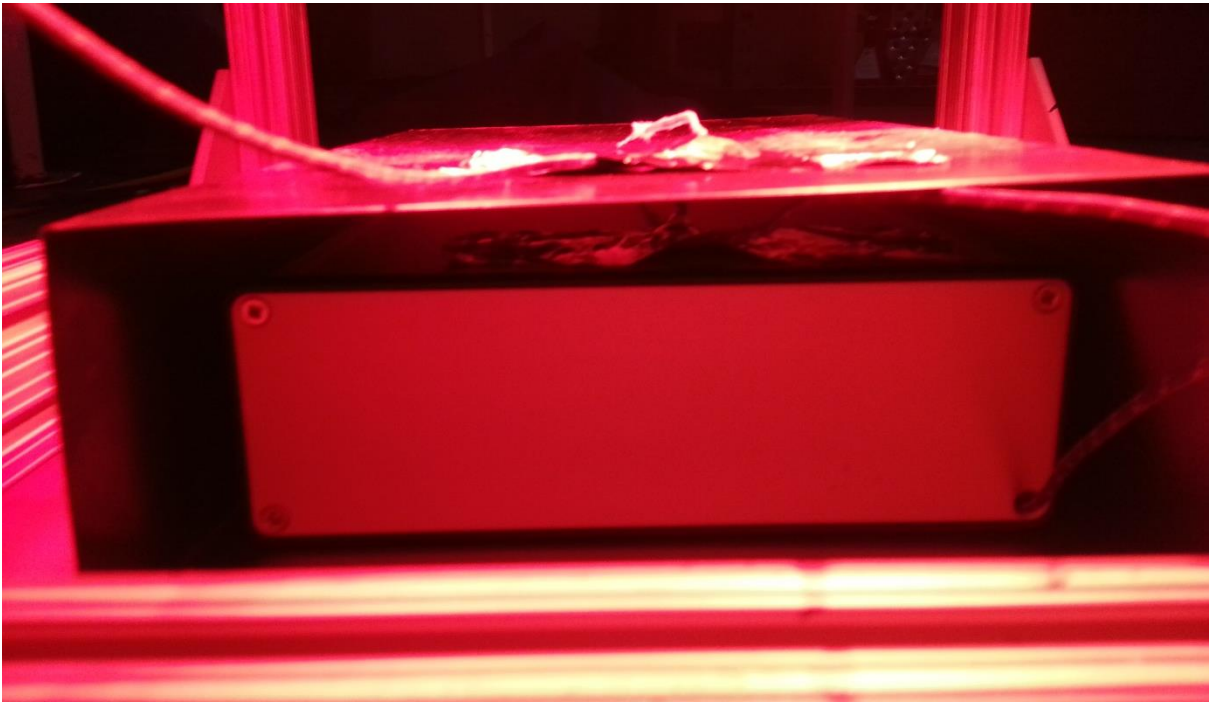


Figure 2-23 Test Setup for Air Pocket Test

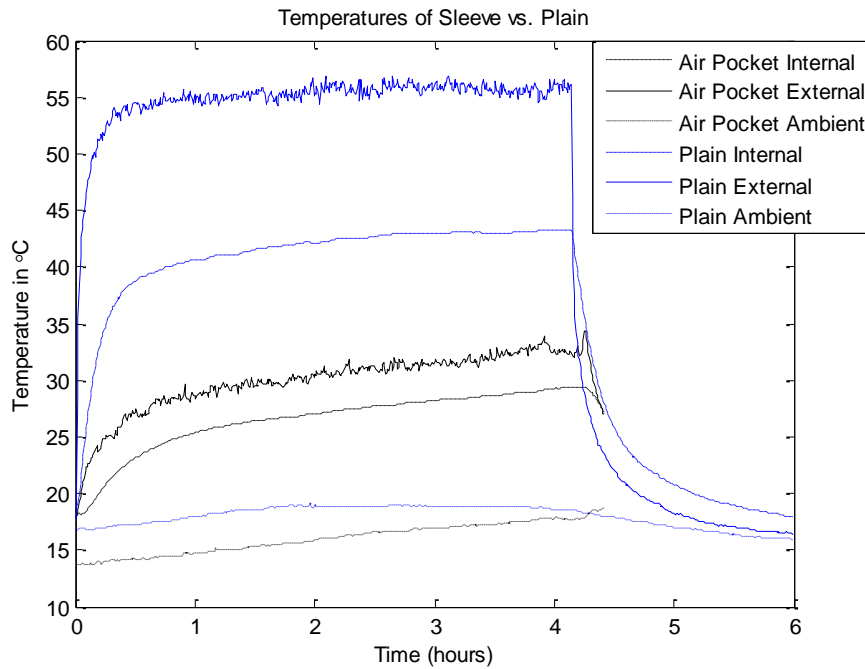


Figure 2-24 Air Pocket vs. No Coating Comparison

This method proved to be the most effective at reducing the effects of solar radiation. This led the design team to explore ways to create a similar air pocket around the GPS receiver box, as described below.

2.5 Hood Design

The success of the air pocket test led to the design of a hood to cover the box. This hood, shown in Figure 2-25, was designed to be removable from the box. To test the effectiveness of the hood, it was mounted under the IR light, as shown in Figure 2-26. Thermocouples were attached to measure the temperature of the top surface of the hood, the bottom surface of the hood, the air inside the hood, and the ambient air temperature. The results are shown in Figure 2-27.



Figure 2-25 Hood Design

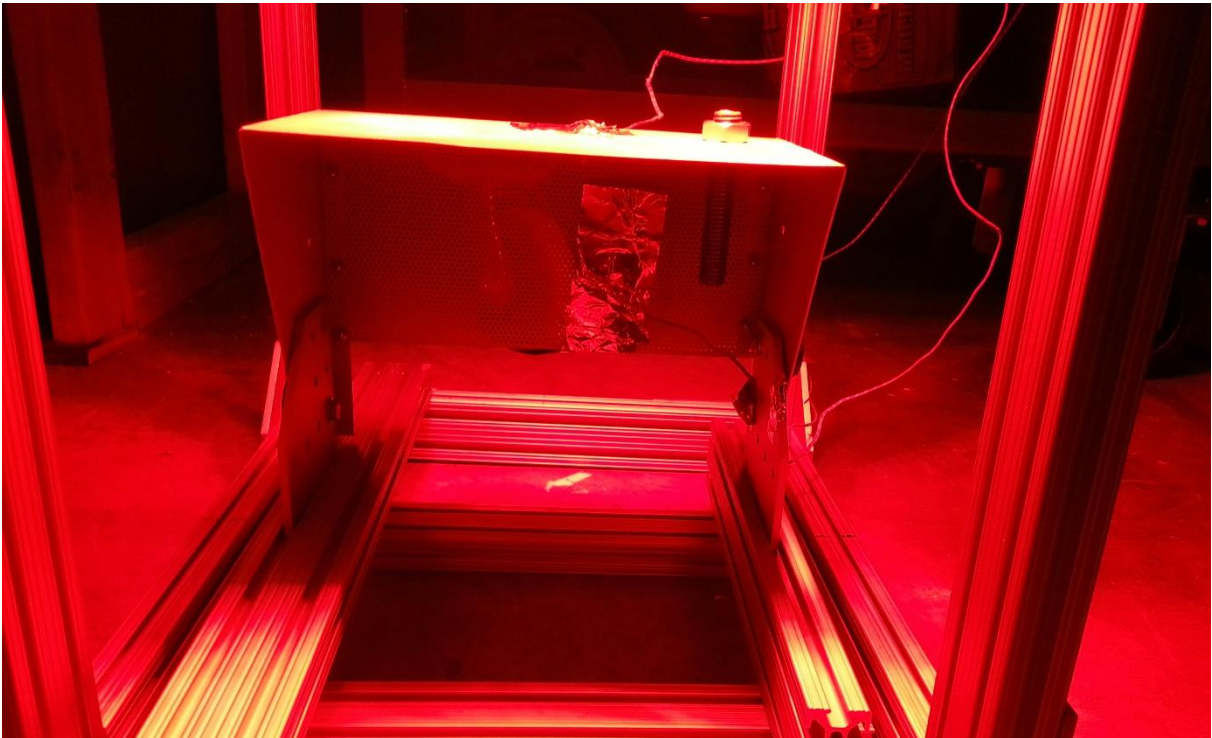


Figure 2-26 Hood Test Setup

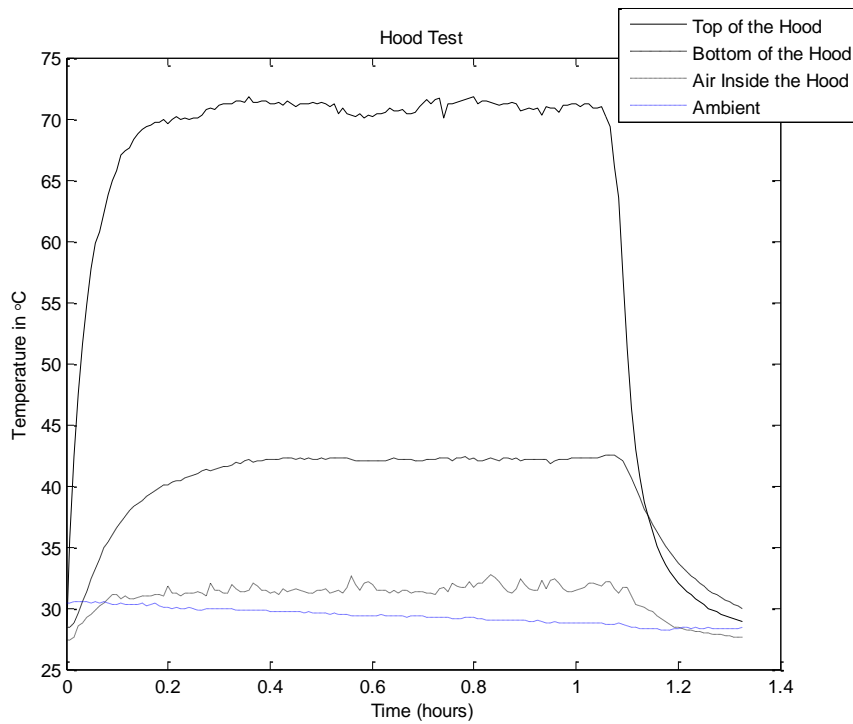


Figure 2-27 Hood Test Results

The results were favorable for the design, as the maximum temperature difference between the air under the hood and the ambient air was 3.7° C, while the top surface of the hood rose to 42.6° C above the ambient temperature.

2.6 Desert Testing

After initial tests were performed in a controlled environment, additional tests were then performed in the actual operating conditions of the of the GPS receiver box. To ensure testing occurred in the worst case scenario, tests at the Yuma Proving Ground in Yuma, Arizona were carried out in the middle of August 2015. During both days of testing, the ambient temperature reached 43.3° C. This is within 4° C of the maximum temperature reached in Yuma in 2015 [18]. Although this is not quite the worst case scenario, it was quite close.

2.6.1 Hood vs. No Hood

The hood design had previously only been tested under the IR light, until it was tested two consecutive days in Yuma. To test the effectiveness of the hood, two empty boxes were mounted to the hood of an SUV with thermocouples measuring temperature at the top and bottom of the interior of the boxes. Only one of the two boxes was equipped with the hood, as shown in Figure 2-28. To simulate operating conditions of the GPS receiver box, the SUV was driven at speeds of 20 m/s or less. Data was also recorded while the SUV was parked for long periods of time. This test was performed on two consecutive days. Figures 2-29 and 2-30 show the results of these two tests.



Figure 2-28 Hood vs. No Hood Test

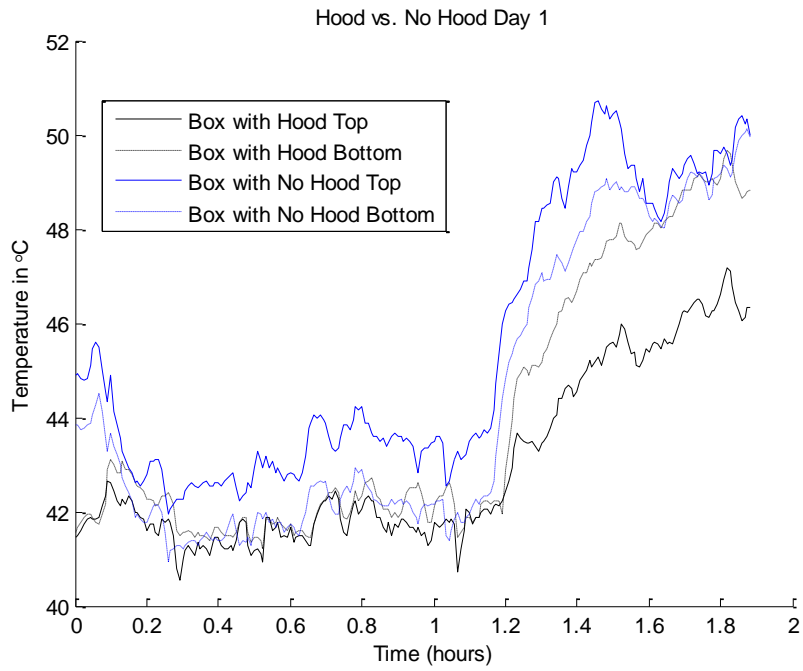


Figure 2-29 Hood vs. No Hood Results Day 1

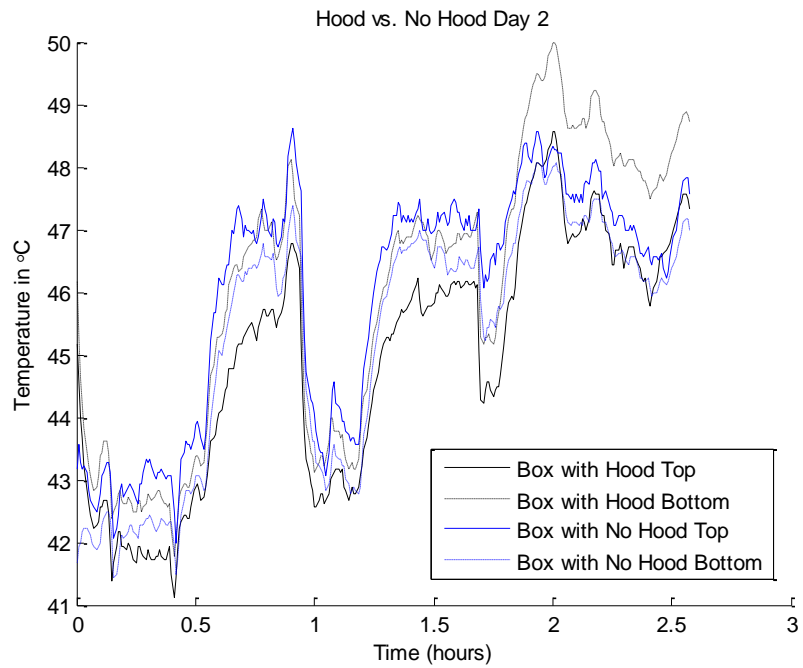


Figure 2-30 Hood vs. No Hood Results Day 2

The results showed that the effectiveness of the hood varied as the direction of the vehicle changed, but overall the hood did provide measurable cooling to the receiver box. The hood usually only kept the top part of the box out of direct sunlight, so the average bottom temperatures for both boxes were within 1° C for both days. For the box without the hood, the top of the box was much hotter than the bottom. For the box with the hood, the bottom was consistently hotter than the top. The average of the top of the box with no hood was 2.4° C and 1° C hotter than the top of the box with the hood.

2.6.2 Powder Coating Test

A powder coating was added to the prototype GPS receiver box to make it more visually appealing. However, it was necessary to test whether the powder coating effected the heating and cooling properties of the box. Two tests were performed for this purpose. The first test was static. Two blank boxes were placed near each other in the desert with a piece of insulation between the box and the ground. Each box had an attached thermocouple to measure the interior temperature. Since the tests were performed on a military base, pictures could not be taken of the test setup. The results of the static test can be seen in Figure 2-31.

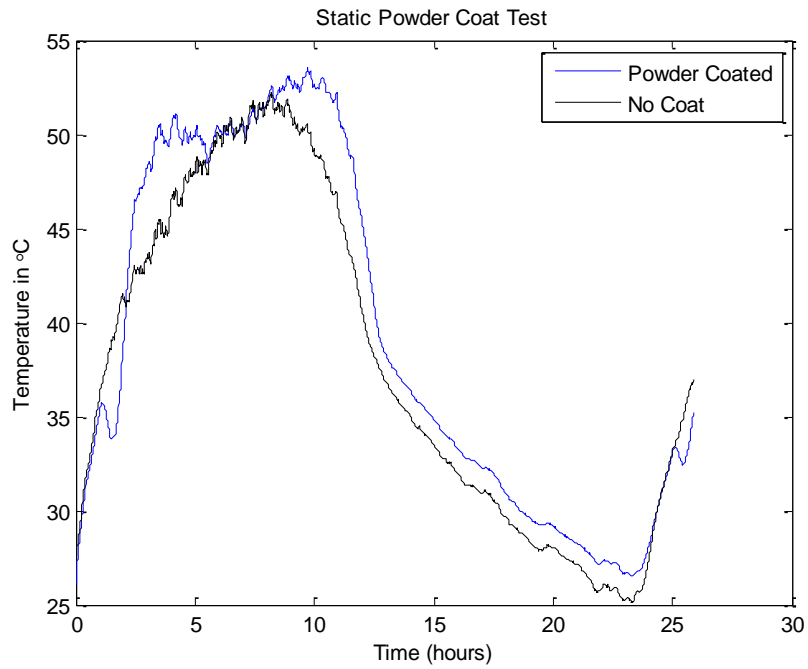


Figure 2-31 Powder Coating Static Test

Another test was performed in which both boxes were placed on the hood of an SUV, in the same manner as the hood test in the previous section. Thermocouples were placed inside the boxes at the top and bottom. The results of this test are shown in Figure 2-32.

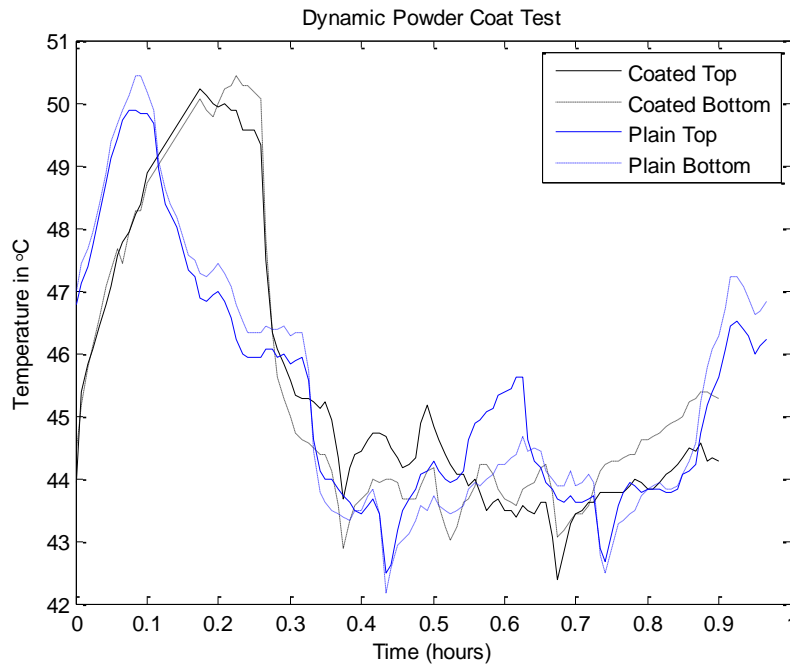


Figure 2-32 Powder Coating Dynamic Test

The results of two tests were somewhat inconclusive. The static test showed that the powder coated box heated up more quickly and cooled down more slowly than the plain box. The powder coated box was an average of 1.4° C hotter than the box with no coating. During the dynamic test, the powder coated box was sometimes hotter and sometimes cooler than the plain box. This was most likely a result of changes in the box orientation and shadows cast as the vehicle moved and changed directions. For this test, the powder coated box was an average of .06° C cooler than the box with no coating. The goal of these tests was to examine the maximum temperatures of the boxes. Since the maximum temperatures of the powder coated box and the plain box do not vary greatly, the powder coating was kept in the final design.

2.6.3 Takachi vs. Hammond Box Comparison

Up to this point, the heat testing had all been done on a Hammond electronics box. However, there was also a Takachi electronic box, which seemed more durable and better suited for a harsh desert environment. To test its performance in the heat, this Takachi box was placed alongside a Hammond box with a hood. The two boxes were placed on the front of an SUV and

driven around the desert. Thermocouples were placed inside the two boxes at the top and bottom of the boxes. The results are shown in Figure 2-33.

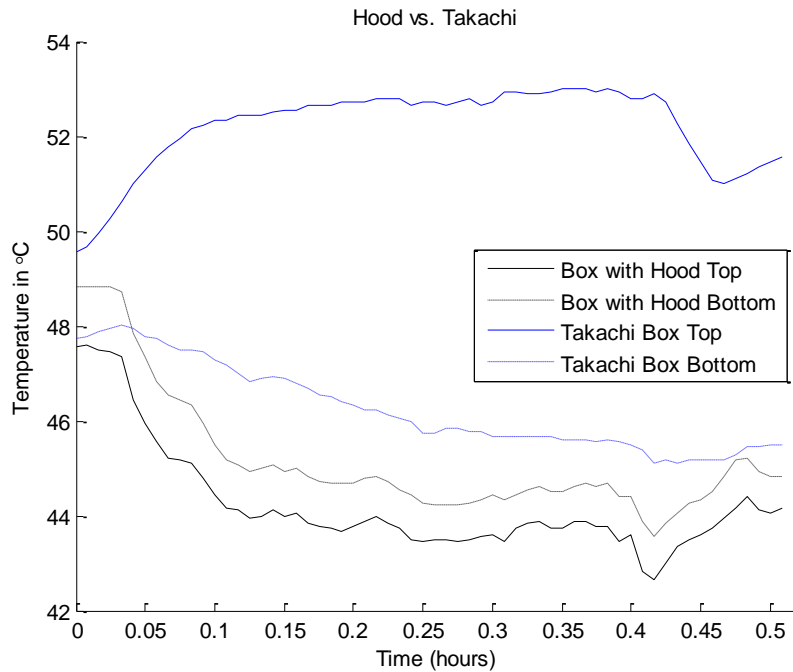


Figure 2-33 Takachi vs. Hammond Box Comparison

The results show the Hammond box with the hood performed better than the Takachi box. The average internal temperature of the Hammond box was 44.7° C, while the average internal temperature of the Takachi box was 49.2° C.

2.6.4 Performance Tests

To test the performance of the boxes in their actual operating conditions, permission was granted to attach a box to a military vehicle while it went through a daily routine. The Takachi box was selected to be attached to the military vehicle, while the Hammond box with the hood was attached to the hood of a rental SUV, which followed the military vehicle for part of the day. Both devices were programmed to run in a loop. This caused the internal components to heat up as they would during operation. Thermocouples were placed inside the Takachi box on the top and bottom of the box. Another thermocouple was placed on the top exterior surface of

the Takachi box. The results are shown in Figure 2-34. While the Takachi box was attached to the military vehicle, the vehicle spent time parked, driving laps around a course, moving from course to course with the SUV following, and some time out of sight of the SUV.

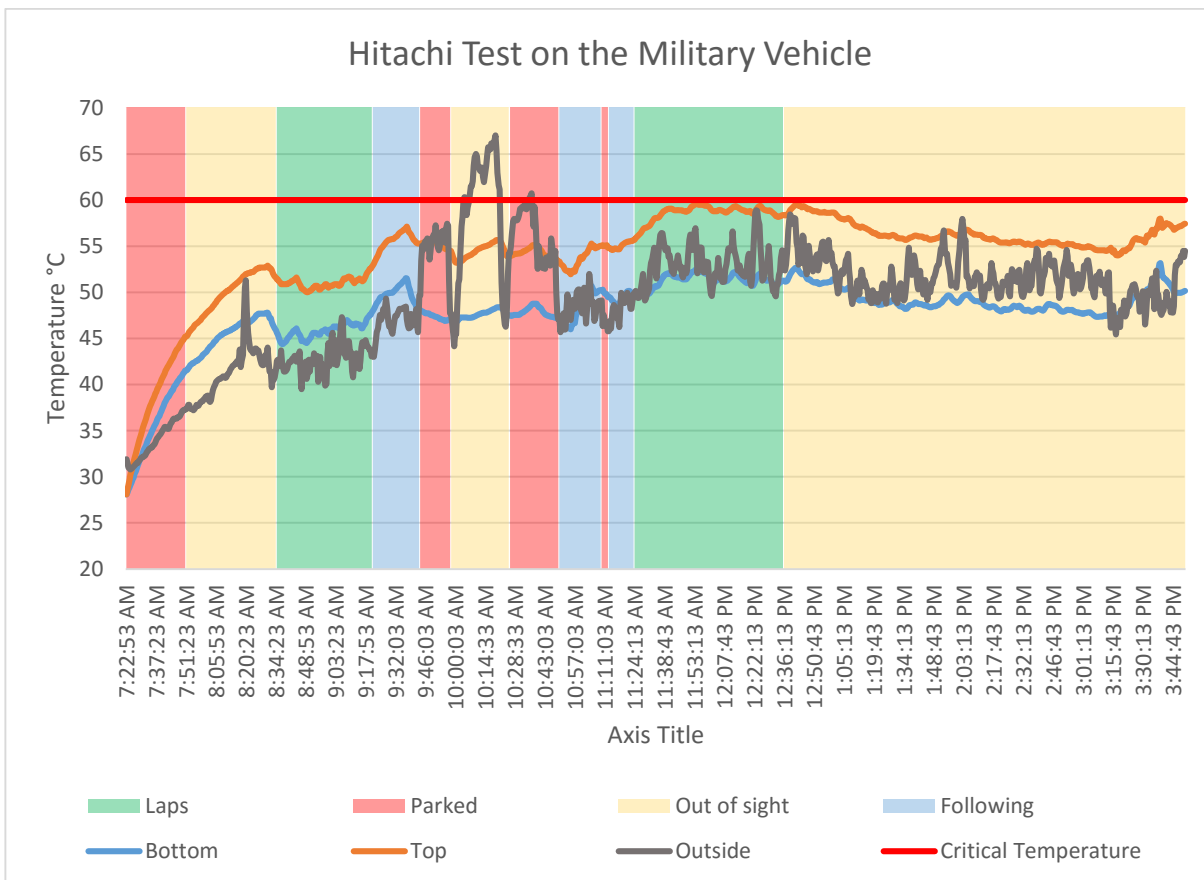


Figure 2-34 Hitachi Box on a Military Vehicle

During the test, it was observed that exhaust fumes were present near where the Takachi box was placed on the military vehicle, and hot air from the exhaust could be felt around the box. This seems to explain the spike in exterior temperature around 10:00 a.m. As a result, the conditions can be considered to be the worst case scenario of operation for the GPS receiver box. The interior temperature of the box rose to 59.6° C, but never rose above the critical temperature of 60° C.

The Hammond box with the hood was placed on an SUV following the military vehicle between

courses. Thermocouples were placed inside the box on the top and bottom. Another thermocouple was placed on the exterior of the box and a fourth thermocouple was placed on the top of the hood. The SUV did not drive laps around the courses, its time was spent parked or driving between courses. The results of the data are shown in Figure 2-35.

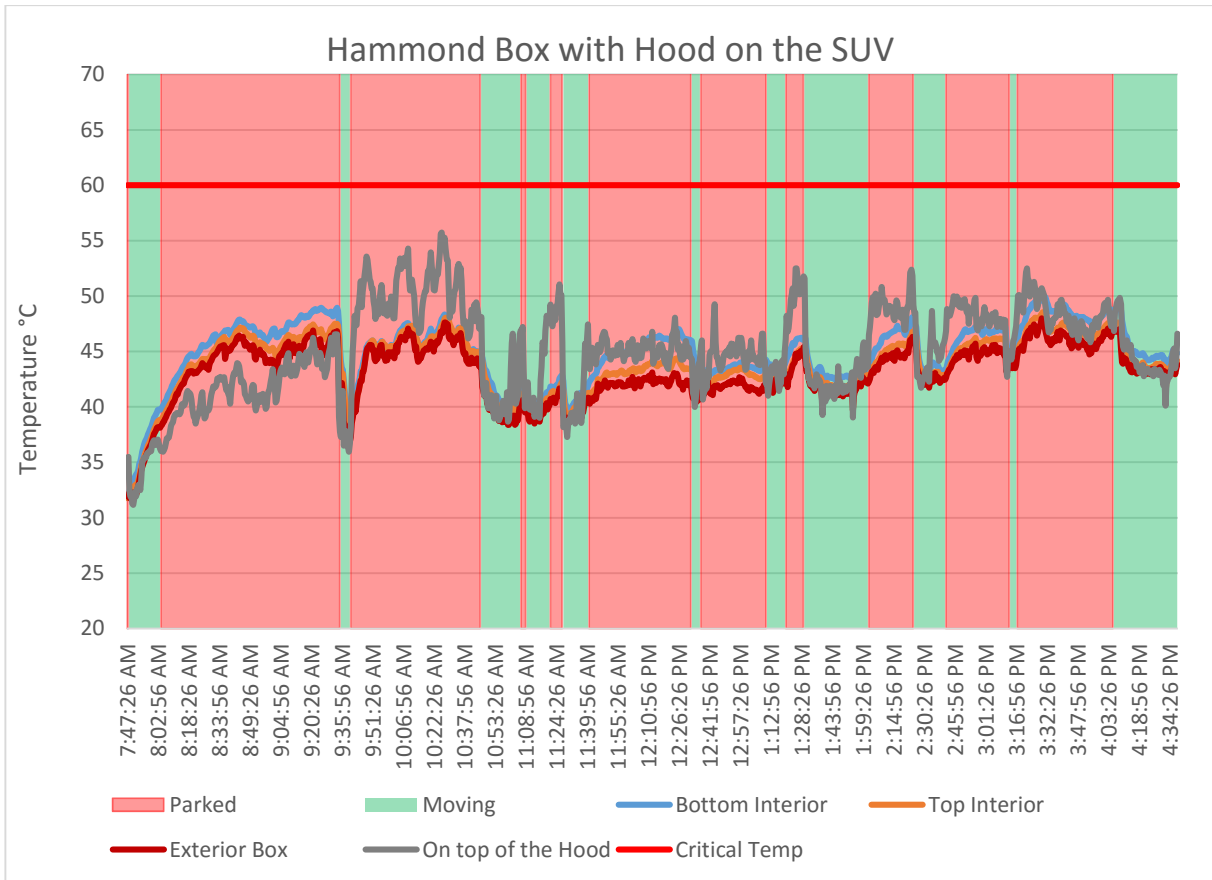


Figure 2-35 Hammond Box with Hood on the SUV

The Hammond box with the hood stayed at a much lower temperature than the Takachi box on the military vehicle. The maximum temperature reached inside the Hammond box was 50° C. It is unclear how much this was affected by the design and how much it was affected by the box not being located near exhaust fumes.

Chapter 3 – Vibration Testing

Another factor that could diminish the performance of GPS receiver box is the effects of vibration in such harsh conditions. Wires becoming disconnected or mechanical failure of any components from vibration could lead to catastrophe. This was a major concern during the design process, and latching electrical connectors were chosen accordingly. Once the system was assembled, it was tested using the V850 Vibration System.

3.1 Test Setup

Vibration testing was performed in accordance with MIL-STD-810G Method 514.6 [11]. There currently is no generalized vibration profile for all tracked vehicles, since these profiles are unique for each vehicle. When this information is not available, Method 514.6 allows for the vibration profile of wheeled vehicles to be used for preliminary testing. Figure 3-1 shows the vibration profile for composite wheeled vehicles, which was used to test the GPS receiver box.

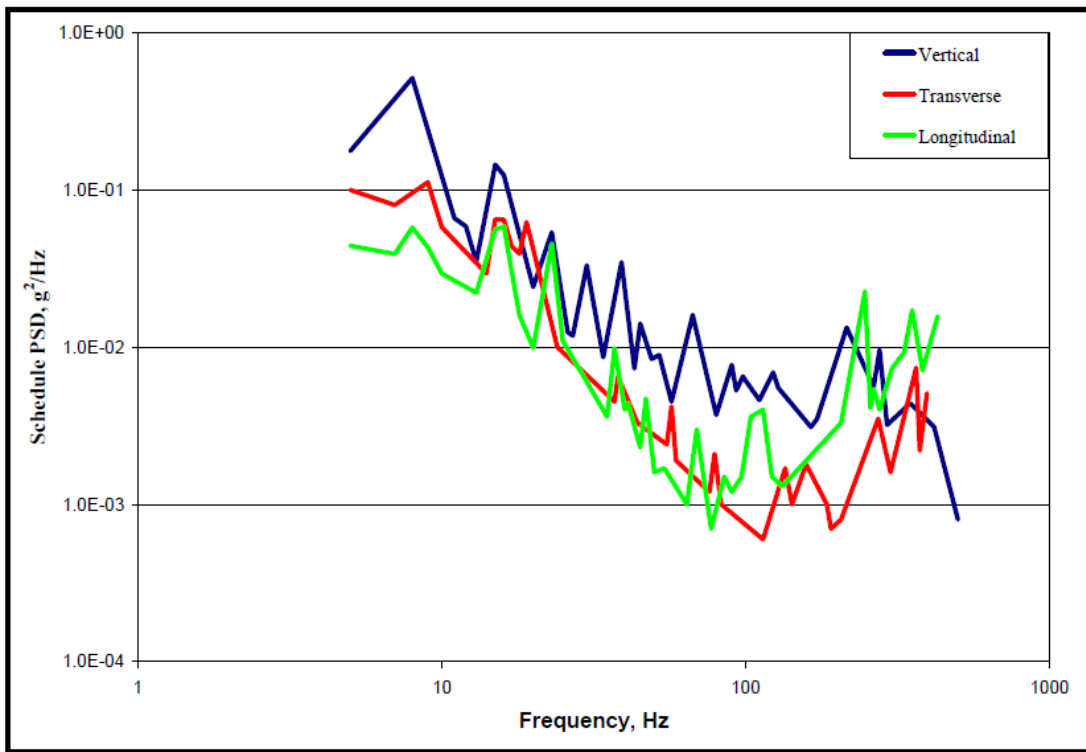


Figure 3-1 Composite Wheeled Vehicle Vibration Exposure

The GPS receiver box was mounted in the vertical, transverse, and longitudinal directions, as shown in Figures 3-2, 3-3, and 3-4. Each direction was given a root mean square of 2.24, 1.48, and 1.90 g's, respectively.



Figure 3-2 Vibration Testing in the Vertical Direction

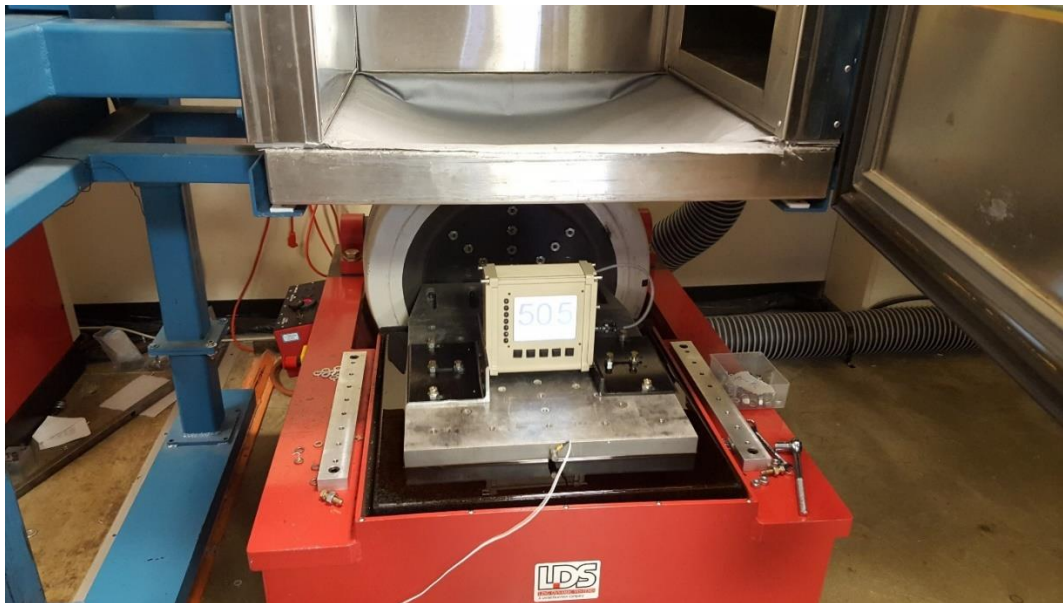


Figure 3-3 Vibration Testing in the Transverse Direction



Figure 3-4 Vibration Testing in the Longitudinal Direction

3.2 Test Results

Before each test, the receiver box was powered on. The GPS software was not completed at this point, so the receiver box was programmed to simply display numbers on the screen in a continuous loop. For the transverse and longitudinal direction, the receiver box was monitored throughout the run make sure the screen was still displaying properly. This was not possible for the vertical direction, as the screen was facing down. For the vertical direction, the screen was observed before and after the test, to ensure everything was running properly. Once all tests were performed, the receiver box was disassembled and each component was examined for broken electrical or mechanical connection.

When the receiver box was disassembled, it was discovered that a hex nut which was used to attach the GPS receiver to the circuit board had come loose and fallen off. This hex nut was replaced with a hex nut with a tooth washer, as shown in Figure 3-5 and 3-6. The tests were then repeated with this replacement, and the receiver box was inspected again. The new hex nuts were all found to be secure.



Figure 3-5 New Nut used for the GPS Receiver



Figure 3-6 The Clamping Nut Holding the GPS Receiver

Chapter 4 – Packaging Solution

Once the testing was complete, a final prototype of the box was assembled. This chapter discusses the components used for packaging, the components on the circuit board, electrical connectors, the battery housing, and the mounting components.

4.1 Packaging

The final box selected for the GPS receiver was a Takachi heat-sink aluminum enclosure with a silicone protector. This box, shown in Figure 4-1, is approximately 213.9 mm by 90.1 mm by 242 mm. The box was then machined, as shown in Figure 4-1, to create holes for the screen, buttons, LED lights, and connection sockets. The silicon protector should provide the box with some additional protection from impact, in case the box is dropped. The sides of the box are designed to increase the surface area exposed to air, allowing the box itself to act as a heat sink for the components inside.

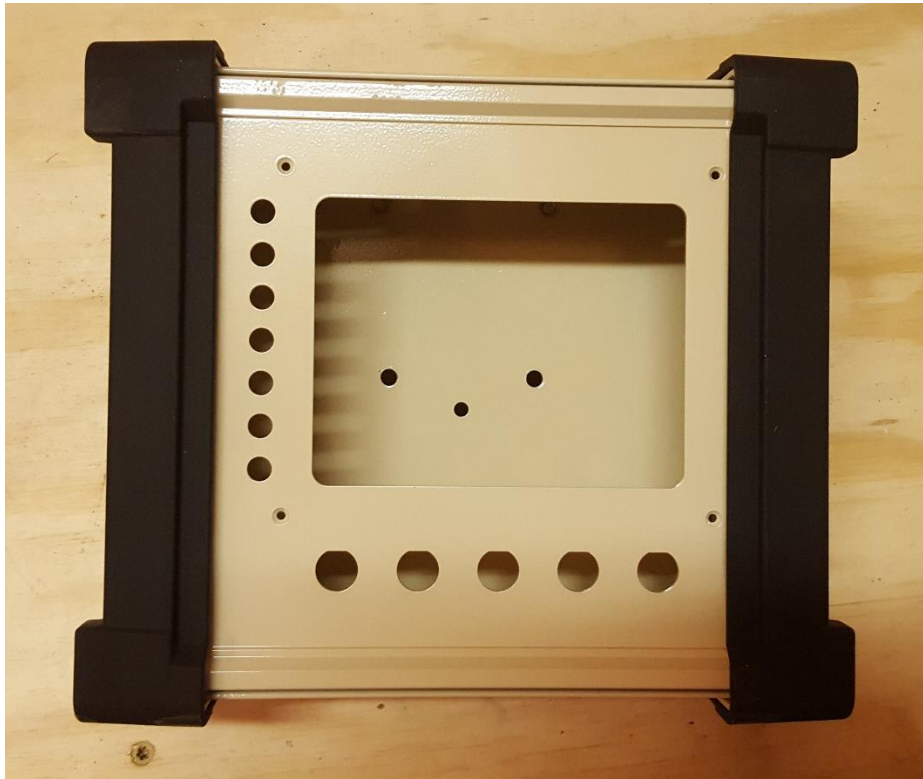


Figure 4-1 Enclosure with Silicon Protector

An LCD screen is mounted to the front of the GPS receiver box using screws and hex nuts with tooth washers. Five pushbuttons are mounted underneath the screen to allow the driver to change settings. Seven LED lights are mounted to the left of the screen as an alert system to the drivers. These lights were clearly visible during all the tests conducted in the desert.

4.2 Circuit Board

Inside the Takachi box, a printed circuit board was placed between slots on the inner wall of the box, as shown in Figure 4-2.

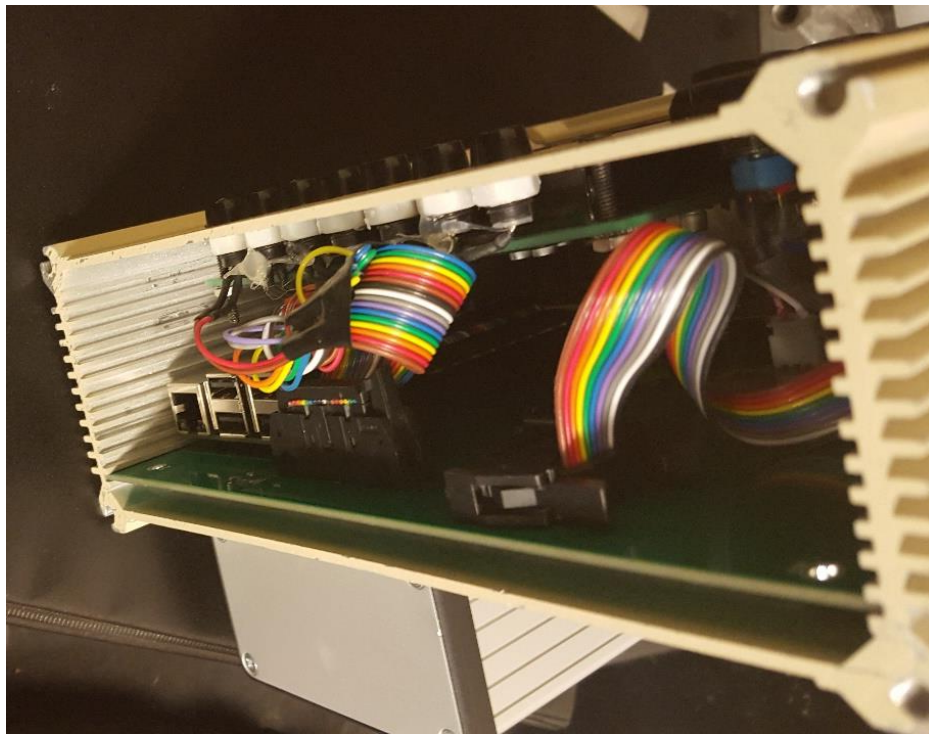


Figure 4-2 Circuit Board in the Box

The GPS receiver, wireless radio module, and computer board are all mounted to the circuit board. As a result of the first vibration test, the GPS receiver is mounted using screws, rubber spacers, and hex nuts with tooth washers as shown in Figure 4-3. The wireless radio is mounted so that the pins are connected to a header and soldered directly to the board, also shown in Figure 4-3. The computer board is mounted to the board with screws and offsets.

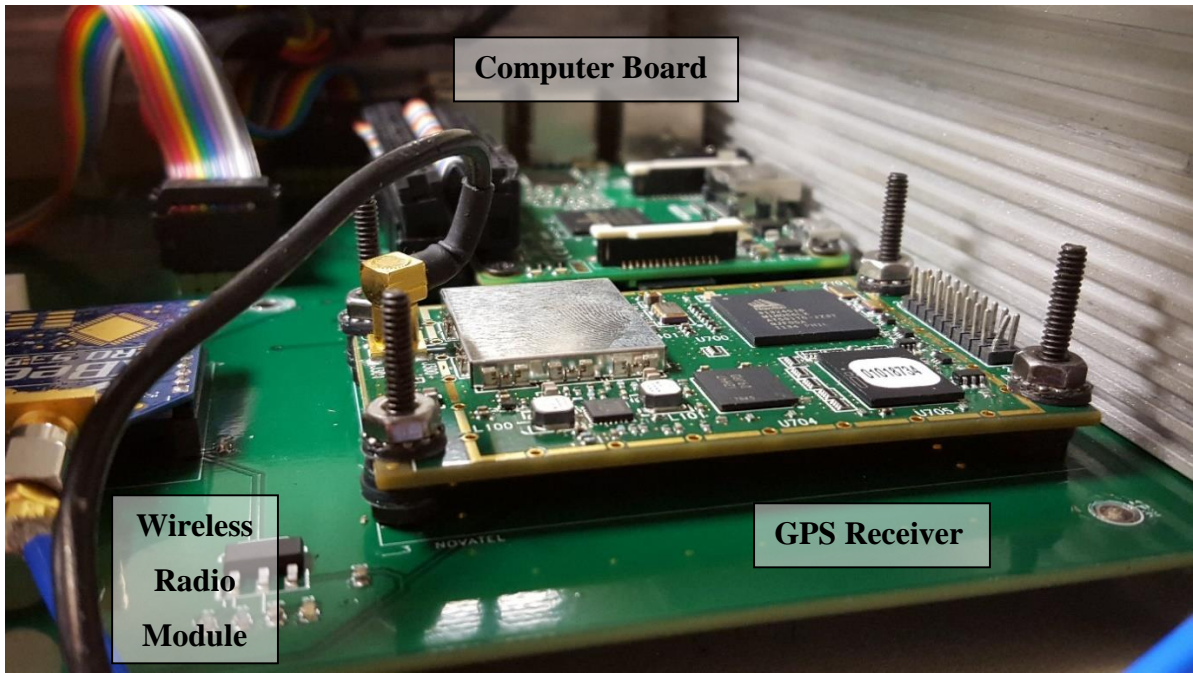


Figure 4-3 Components on the Board

4.3 Connectors

Due to the potentially catastrophic effects of vibration induced failure, extra attention was given to selecting electrical connectors. Connections within the box and connections on the exterior of the box are subject to the effects of vibration, and could be detrimental if they become loose. Within the box, every component must be connected to the circuit board. Both the radio module and the GPS receiver are wired directly to the circuit board through a header. The computer board, LED lights, LCD screen, battery, screen backlight, and push buttons are all connected through wires with various latching connections as shown in Figures 4-4, 4-5, 4-6, and 4-7.

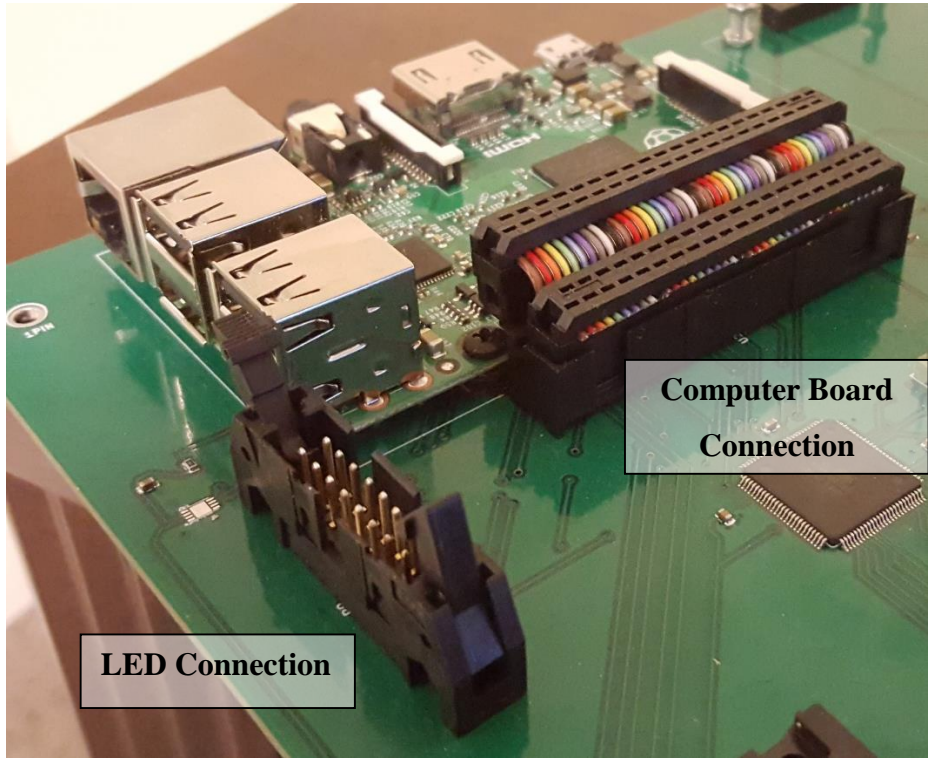


Figure 4-4 LED Lights and Computer Board Connection

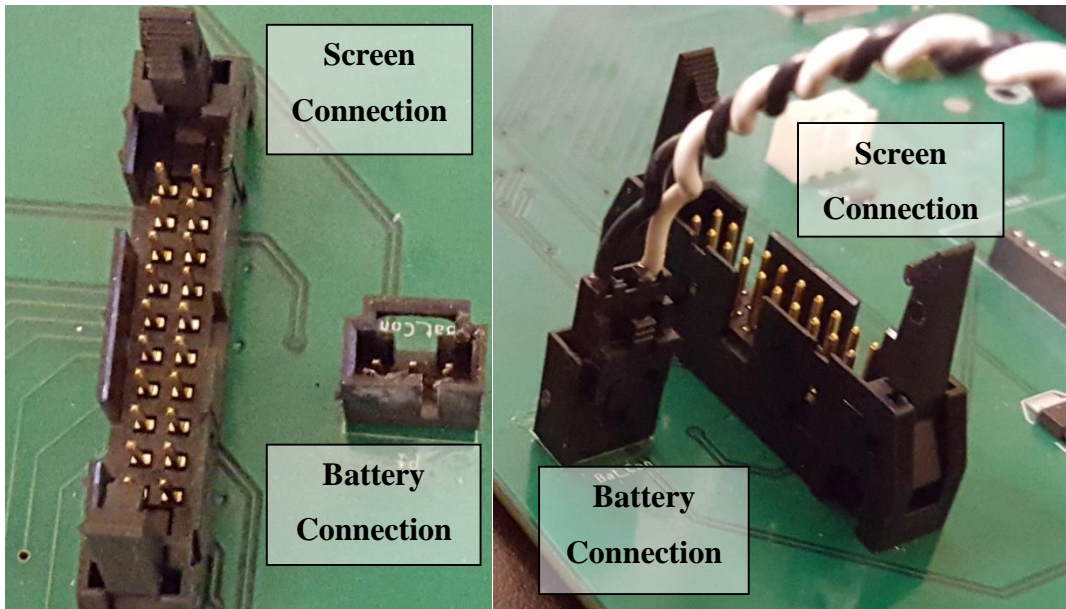


Figure 4-5 Screen and Power Latching Connections

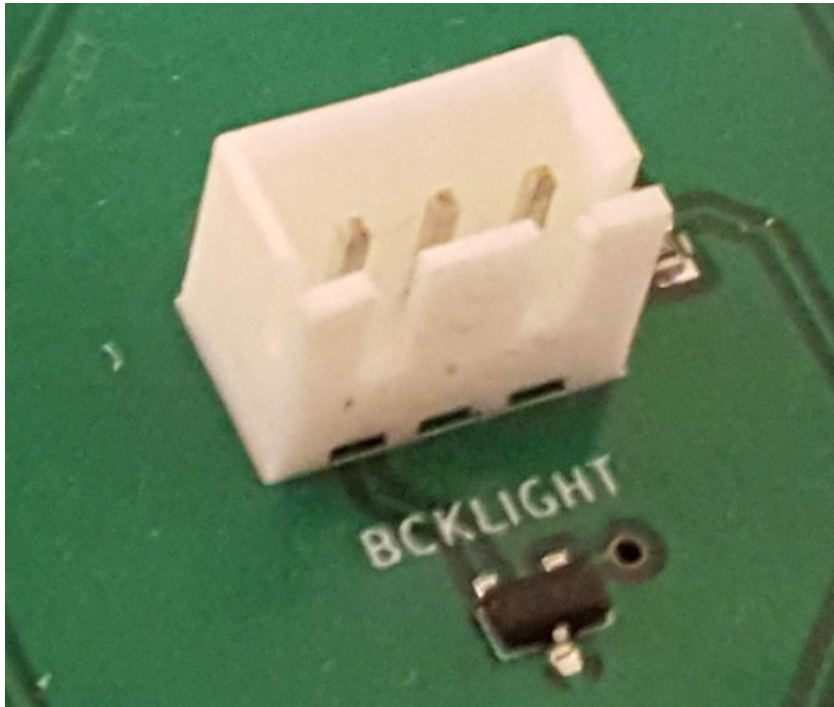


Figure 4-6 Latching Connection for Screen Backlight

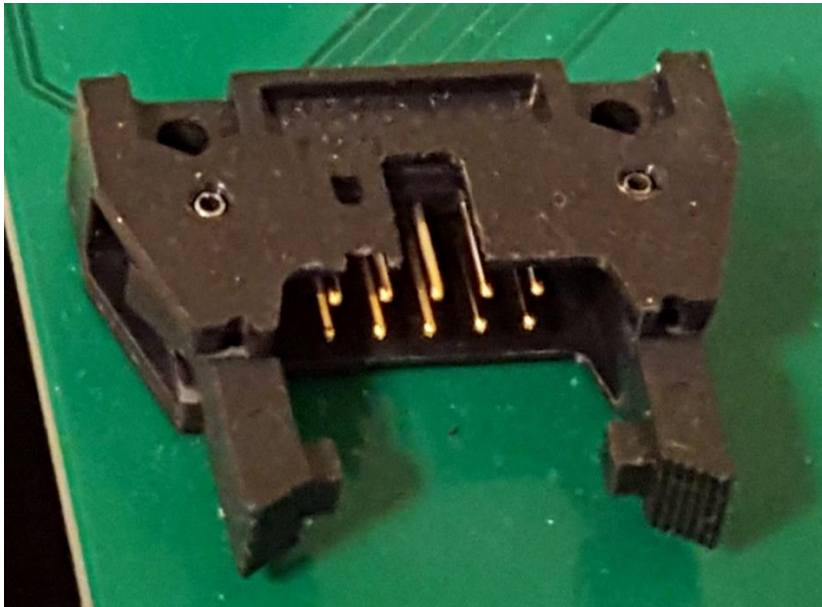


Figure 4-7 Latching Connection for Push Buttons

Along with being connected to the circuit board, these internal components must also connect to components outside of the box. The GPS receiver and the radio module must each connect to an antenna on the exterior of the box. The battery, located on the exterior of the box, must also be able to provide power to the inside of the box. Figure 4-8 shows the interior side wall of the box where these components are wired to connect with exterior components. The power connection port is secured using four screws and bolts. The power supply travels from this port to the power button, which is then connected to the circuit board. This power button is threaded, which allows it to clamp onto the sidewall, securing it and sealing the hole from dust contamination. Similarly, the GPS receiver and the radio module are both wired to threaded ports, which also use threads to clamp the ports to the side wall.

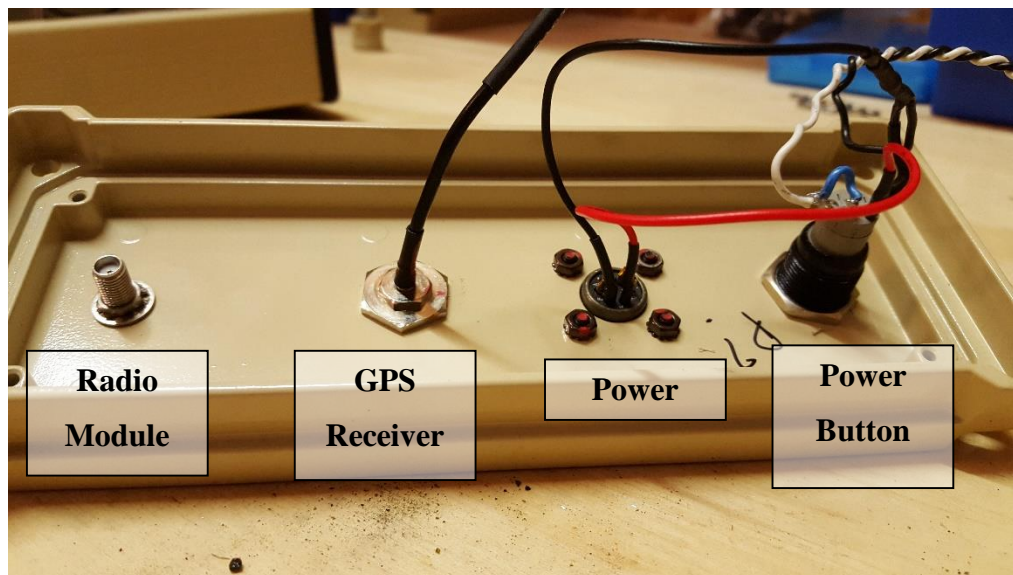


Figure 4-8 Interior Side Wall with Connection Ports for Exterior Components

Figure 4-9 shows the exterior of the side wall where external components connect to the box. The radio antenna screws directly to the port shown, while the GPS antenna connects to the port through a cable with threaded ends. The power supply is connected with a cable that can be twisted to lock the connection in place. These connectors were selected specifically to stay secure while experiencing vibrations.

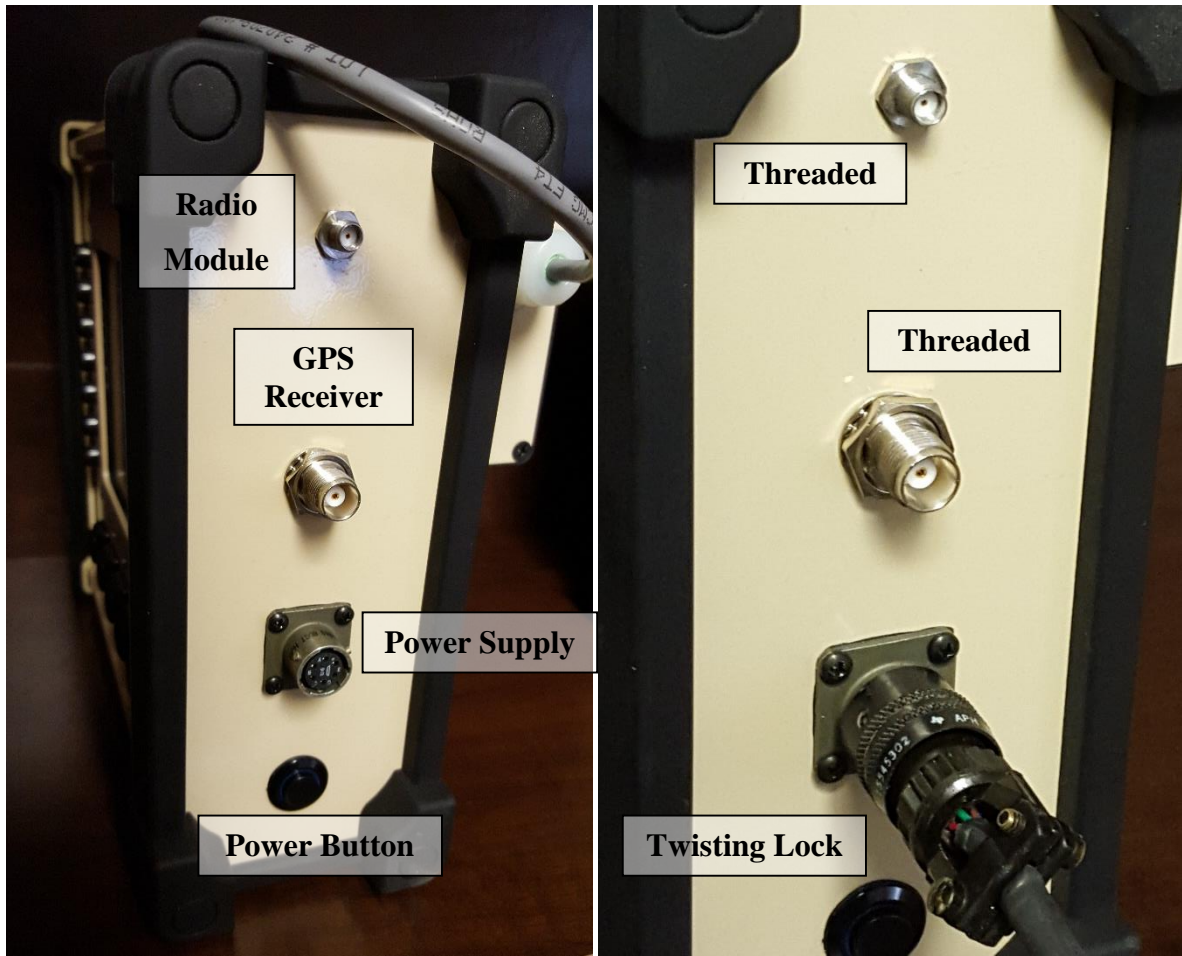


Figure 4-9 Exterior Connection Ports

The port attached to the GPS antenna is connected to the GPS receiver through the cable shown in Figure 4-10. The placement of the GPS receiver wedges this cable between the GPS receiver and the board, making the connection more secure and less susceptible to the effects of vibration. The power supply connects to the circuit board using the latching connector previously shown in Figure 4-5. The radio attaches to the port with the radio antenna through a cable threaded on both ends. All of these connections should provide extra protection from the cables becoming disconnected as a result of vibration.

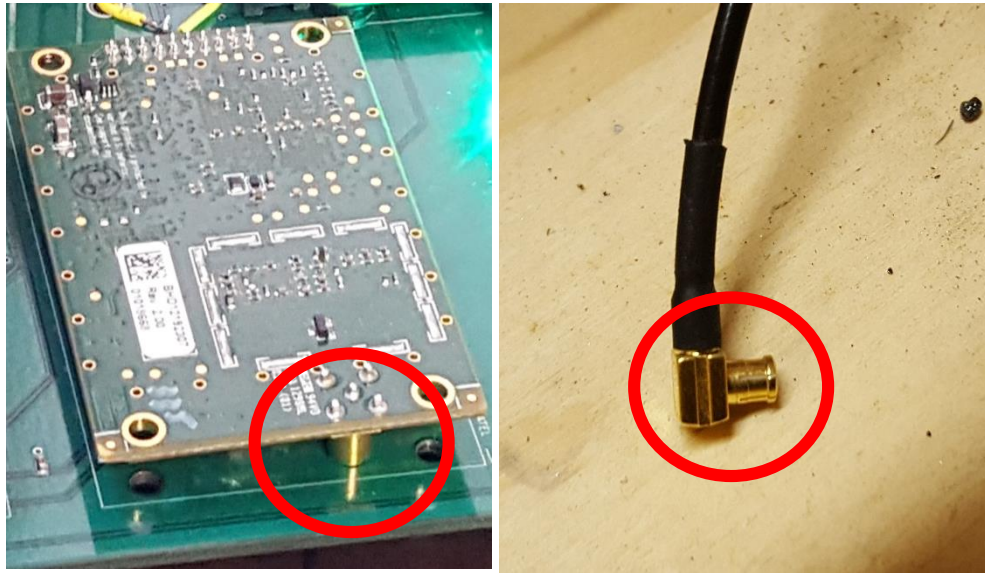


Figure 4-10 Connection from GPS Receiver to Antenna

4.4 Battery

One of the crucial challenges for this project is finding a power supply capable of providing enough power, while still being self-contained within the GPS receiver box. To do this, two 7.4 V 5200 mAh rechargeable battery packs are used. To reduce heating effects, the battery packs are placed in a separate electronic box shown in Figures 4-11, 4-12, and 4-13. The battery box is filled with insulating foam to keep the batteries in place as shown in Figure 4-11. The battery box attaches to the GPS receiver box using bolts as shown in Figure 4-12 and 4-13. Spacers provide a gap between the two boxes, which will prevent the receiver box from acting as a heat sink for the battery box. There is a ledge on the back of the receiver box, beneath the battery box to stabilize it. This design allows for the power supply to be attached to the receiver box, without providing additional heating or requiring a larger box to be used.



Figure 4-11 Battery Box with Internal Foam

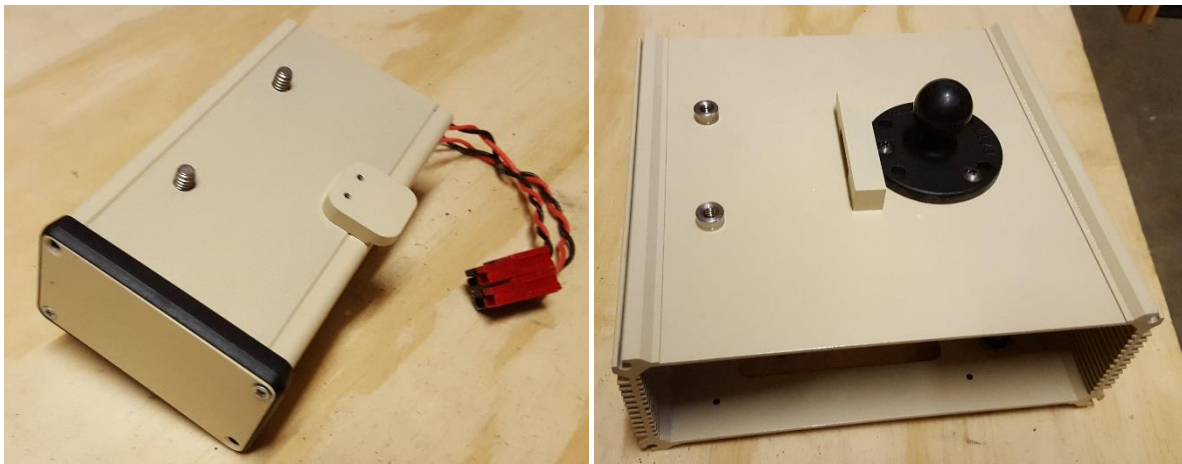


Figure 4-12 Battery Box Before Mounting to the Receiver Box



Figure 4-13 Battery Box Mounted to the Receiver Box

4.5 Mounting System

With the box assembled, the final element needed is a way to mount the box to the military vehicle. To do this, a ball mount is attached to the back of the GPS receiver box using screws and hex nuts with tooth washers. This will help the mount remain secure when the box vibrates. A double socket arm clamps to this ball mount at one end and another ball mount at the other end. This other ball mount can be bolted in to a handle on the exterior of the military vehicle. This mounting system, shown in Figure 4-14, was used when the box was mounted on the military vehicle during desert testing, and held in place throughout the duration of the day. Alternatively, a magnetic ball mount can also be used in place of this bolted ball mount.



Figure 4-14 Mounting System

Chapter 5 – Summary and Conclusions

5.1 Summary and Conclusions

Applications of personal handheld electronic devices, such as GPS receivers, have increased in recent years. As a result, it is required for such devices to be able to operate in a wide variety of harsh environmental conditions. A desert environment poses several threats to electronic devices, such as heat, vibration, and dust. This thesis details the tests performed and resulting design choices for ensuring that a GPS receiver would be able to operate in the midst of these harsh conditions. It was shown that solar radiation posed the greatest threat to the life and performance of the GPS receiver box. The effectiveness of several passive cooling methods, such as reflective tape, insulating coating, and a hood design were tested and the results have been detailed. A hood design was shown to be effective in protecting the GPS receiver box from solar radiation, but it was also shown that this design may not be necessary for a larger box. Vibration testing showed that using hex nuts with tooth washers held components more securely than regular hex nuts. The final individual components used to counteract the harsh environmental effects have also been discussed.

5.2 Future Work

Although many tests have already been performed, several more need to be conducted to ensure the maximum performance of the box. Some of these tests will use the test setup previously described in this work, with some modifications. Other tests still need to be done in the actual environment in which the GPS receiver box will operate.

5.2.1 Lab Testing

The lab tests conducted so far have focused on whether the box is capable of performing under the harsh heat and vibrations experienced in a desert environment. However, more tests still need to be performed to examine how long term exposure to these effects will impact the expected life of the components in the GPS receiver box. To do this, the test setup with the IR light will be used in a heated chamber, which will allow the ambient temperature to be

maintained around the approximate ambient temperature experienced in the desert. With the correct ambient temperature and radiative heat load, the box will undergo heated cycles meant to simulate days spent in the desert. Once the GPS receiver box has undergone multiple consecutive days of testing, the internal components will be examined along with the overall performance of the box. Similarly, the box will also need to undergo extended vibration testing to examine the effects of vibration over a long period of time. The final environmental condition which has yet to be tested, is the effects of dust on the GPS receiver box. To examine this, dust from the desert will be used for a variety of tests. To test how well it is sealed from dust, the GPS receiver box will be intentionally covered in dust. After this test, the box will be taken apart and examined for dust particles on the interior. Along with testing the overall GPS receiver box, the performance of individual components will also be examined in the presence of dust. The various electrical connectors will be disconnected, dipped in the dust, reconnected, and their performance will be examined. Dust will also be applied to the circuit board to examine the magnitude of the effects from different amounts of dust.

5.2.2 Desert Testing

Despite all the lab testing that has been performed and will continue to be performed, the GPS receiver box still needs to undergo testing in its actual operation environment. The military vehicle on which the GPS receiver box will be mounted could create environmental challenges previously unaccounted for. Heat could radiate off of the vehicle itself, causing the internal box temperature to reach levels higher than expected. This could require a change of internal components, or the use of a hood similar to the one previously examined. As previously discussed, each tracked vehicle provides its own unique vibration profile. Ultimately, the box will have to operate in these conditions for an extended period of time, before the design will be completely finalized.

References

- [1] F. A. L. Souza, P. C. T. Pereira, H. de Paula, B. J. C. Filho and A. V. Rocha, "Motor drive systems reliability: Impact of the environment conditions on the electronic component failure rates," *Industry Applications Society Annual Meeting, 2014 IEEE*, Vancouver, BC, 2014, pp. 1-8.
- [2] "Reliability Design Thermal Applications". 1978, MIL-HDBK-251, Department of Defense.
- [3] "F. A. L. Souza, H. de Paula, B. J. C. Filho, A. V. Rocha and G. I. C. Lobato, "Influence of environmental factors on the reliability of electronic components used in motor drive systems," *Power Electronics Conference (COBEP), 2013 Brazilian*, Gramado, 2013, pp. 942-949.
- [4] Bing, G., Javed, W., Figgis, B. W., and Mirza, T. "Effect of Dust and Weather Conditions on Photovoltaic Performance in Doha, Qatar," *2015 First Workshop on Smart Grid and Renewable Energy*, Doha, Qatar, pp. 1-6.
- [5] Keranen, E. D., 2009, "Special Report: Effects of Dust on Computer Electronics, And Mitigating Approaches", Computer Dust Solutions, LLC, Hancock, Michigan, http://www.computerdust.com/downloads/special_report_on_the_effect_of_dust_on_electronics.pdf
- [6] Brumfiel, G., 2010, "Swirling Dust Shocks Physicists," International Weekly Journal of Science, <http://www.nature.com/news/2010/100411/full/news.2010.174.html>
- [7] Y. S. Chen, H. K. Lai, T. C. Lin, P. H. Chang and M. U. Jen, "Analyses of printed circuit boards subjected to vibration loadings under various clamping types and reinforced ribs," *Microsystems, Packaging, Assembly and Circuits Technology Conference (IMPACT), 2015 10th International*, Taipei, 2015, pp. 378-381.

- [8] Williamson, A. G., Allen, R. M., McNeill, R. G., Williamson, and Wallace, K. L., 2001 “Cooling of Telecommunications Enclosures in Tropical & Desert Environments,” No. 484, *Telecommunications Energy Conference, INTELEC 2001*, Edinburgh, UK, pp. 101-108.
- [9] R. C. Chu, "Advanced cooling technology for leading-edge computer products," *Solid-State and Integrated Circuit Technology, 1998. Proceedings. 1998 5th International Conference on*, Beijing, 1998, pp. 559-562.
- [10] Bergman, T. L., Lavine, A. S., Incropera, F. P., and DeWitt, D. P., 1978, *Fundamentals of Heat and Mass Transfer, 7th Edition*, McGraw-Hill, New York.
- [11] “Environmental Engineering Considerations and Laboratory Tests,” 2008 MIL-STD-810G, Department of Defense.
- [12] <http://www.speedymetals.com/information/Material26.html>
- [13] Bergstrom, D., Powell, J., and Kaplan, A. F. H., 2006, “The Absorptance of Steels to Nd:YLF and Nd:YAG Laserlight at Room Temperature,” *Applied Surface Science*, (253), 5017-5028
- [14] Abdul Karim, S. A. and Mahinder Singh, B. S., 2014, “Global Solar Radiation Modeling Using Polynomial Fitting,” *Applied Mathematical Sciences*, **8** (8), pp. 367-378.
- [15] http://www.wunderground.com/history/airport/KNYL/2015/8/19/DailyHistory.html?req_city=&req_state=&req_statename=&reqdb.zip=&reqdb.magic=&reqdb.wmo
- [16] “Guide to Meteorological Instruments and Methods of Observation,” 2006, WMO-No. 8, World Meteorological Organization, Geneva, Switzerland.
- [17] <http://www.lizardskin.com/car-ceramic-insulation.html>
- [18] <https://weatherspark.com/averages/31083/Yuma-Arizona-United-States>

Appendix A

MATLAB Programs

CalculatePowerValues.m

```
clc
clear all
close all
%% Import data from spreadsheet
%% Import the data
height = 18;
wind = 0;
if height == 12;
    [~, ~, raw] =
xlsread('E:\YUMA\02_08_2016_SteelPlate_12in_sand_nofan.xlsx','02_08_2016_SteelPlate_
12in_sand','E2:H2922');
    Change = 741;
    heightnum = 2;
    StableRange = 379:Change-1;

elseif height == 18;
    [~, ~, raw] =
xlsread('E:\YUMA\02_15_2016_SteelPlate_18in_sand_nofan.xlsx','02_15_2016_SteelPlate_
18in_sand','E2:H1732');
    Change = 984;
    heightnum = 3;
    StableRange = 865:Change-1;
    heightnum = 3;

elseif height == 24;
    [~, ~, raw] =
xlsread('E:\YUMA\12_01_2014_SteelPlate_24in.xlsx','12_01_2014_SteelPlate_24in','E2:H24
91');
    Change = 2408;
elseif height == 6;
    [~, ~, raw] =
xlsread('E:\YUMA\02_01_2016_SteelPlate_6in_sand_nofan.xlsx','02_01_2016_SteelPlate_6i
n_sand_', 'E2:H934');
    Change = 503;
    heightnum = 1;
    StableRange = 241:Change-1;
else error('Height not recorded')
end
```

```

%% Create output variable
data = reshape([raw{:}],size(raw));

%% Allocate imported array to column variable names
T1 = smooth(data(:,1));
T2 = smooth(data(:,2));
T3 = smooth(data(:,3));
T4 = smooth(data(:,4));

%% Clear temporary variables
clearvars data raw;
%% Constants
g = 9.81; %acceleration due to gravity (m/s^2)
A = 8*6*0.00064516; %Area of top surface (m^2)
P = (8+6)*2*0.0254; %Perimeter of top surface (m)
L = A/P; %Effective Length of Plate (m)
sigma = 5.670373*10^-8; %J/K^4*m^2*s
ep = .8;
dt = 30;
VolumeIn = .25*6*8; %in^3
Volume = VolumeIn*.0000163871;
Density = 7832; %Kg/m^3
Density2 = 7870; %Kg/m^3
m2 = Volume*Density;
n = 1.540124; %Kg
Area = 0.03096768; %m^2
Cp = 486*m2; %J/K
absorp = .62;

for n = 1:length(T1)
    time(n) = 30*(n-1);
end
%% Dividing temperature Data into categories
T1F = T1.*9/5+32;
T2F = T2.*9/5+32;
T3F = T3.*9/5+32;
T4F = T4.*9/5+32;
T1Heat = T1(1:Change);
T2Heat = T2(1:Change);
T3Heat = T3(1:Change);
T4Heat = T4(1:Change);
T1Cool = T1(Change+1:length(T1));

```

```

T2Cool = T2(Change+1:length(T2));
T3Cool = T3(Change+1:length(T3));
T4Cool = T4(Change+1:length(T4));
TAveCool = (T1Cool+T2Cool)./2;
timeheat = time(1:Change);
timecool = time(Change+1:length(T4));
TempDiff = T1-T4;
TempDiffHeat = TempDiff(1:Change);
TempDiffCool = TempDiff(Change:length(TempDiff));

```

%% Simulation

```

TSurface(1)= T1Heat(1);
Tave = (T1+T2)./2;
TempChange(1) = (T1Heat(2)-T1Heat(1))/(time(2)-time(1));

```

```

[~, ~, raw] = xlsread('E:\YUMA\HeatTransferProperties.xlsx','Air','A2:H42');

```

%% Create output variable

```

data = reshape([raw{:}],size(raw));
%% Allocate imported array to column variable names
TAirData = data(:,1); %Temperature values of Air in C
rhoAirData = data(:,2); %Density values of air in kg/m^3
KAirData = data(:,4); % Thermal conductivity of air in W/mK
alphaAirData = data(:,5); %in m^2/s
DynViscAirData = data(:,6); %Dynamic viscosity of air in Ns/m^2
KinViscAirData = data(:,7); %Kinematic viscosity of air in m^2/s
PrAirData = data(:,8); %Prandtl Number of air

```

%% Clear temporary variables

```
clearvars data raw;
```

```
n = 1;
```

```
while n <= Change-1 %length(T1)-1 %
```

```
    dt(n) = time(n+1)-time(n);
```

```
    Tf(n) = (T4(n)+T1(n))/2;
```

```
    xA(n) = find(TAirData>Tf(n), 1, 'first') ;
```

```
AirPercentage(n) = (Tf(n)-TAirData(xA(n)-1))/(TAirData(xA(n))-TAirData(xA(n)-1));
```

%Used to interpolate air values

```
rho(n) = AirPercentage(n)*(rhoAirData(xA(n))-rhoAirData(xA(n)-1))+rhoAirData(xA(n)-1);
```

%Finds density of air given the temperature

```
mu(n) = AirPercentage(n)*(DynViscAirData(xA(n))-DynViscAirData(xA(n)-1))+DynViscAirData(xA(n)-1); %Finds dynamic viscosity of air given the temperature
```

```
nu(n) = AirPercentage(n)*(KinViscAirData(xA(n))-KinViscAirData(xA(n)-1))+KinViscAirData(xA(n)-1); %Finds kinematic viscosity of air given the temperature
```

```

K(n) = AirPercentage(n)*(KAirData(xA(n))-KAirData(xA(n)-1))+KAirData(xA(n)-1);
%Finds conductivity of air given the temperature
alpha(n) = AirPercentage(n)*(alphaAirData(xA(n))-alphaAirData(xA(n)-1))+alphaAirData(xA(n)-1); %Finds alpha of air given the temperature
Pr(n) = AirPercentage(n)*(PrAirData(xA(n))-PrAirData(xA(n)-1))+PrAirData(xA(n)-1);
%Finds Prandtl number of air given the temperature
Beta(n) = 1/(Tf(n)+273);
DeltaT(n) = (T1(n)-T4(n));
Ra(n) = g*Beta(n)*abs(DeltaT(n))*L^3/(alpha(n)*nu(n));
Nu(n) = .54*Ra(n)^(1/4);
H(n) = K(n)*Nu(n)/L*A; % W/K*m^2 or W/C
RadiationLoss(n) = ep*A*sigma*((T4(n)+273)^4-(T1(n)+273)^4);
QConv(n) = H(n)*(T4(n)-T1(n)); % Watts*m^2

Tdot(n) = (T1(n+1)-T1(n))/dt(n);
Power(n) = (Cp*Tdot(n)-RadiationLoss(n)-QConv(n))/absorp;

n=n+1;

end
figure
timeplot = time/3600;
plot(timeplot(1:length(Power)),Power/A,'k');
title(['Calculating Radiative Load for Height ',num2str(heightnum)])
xlabel('Time (hours)')
ylabel('Power (Watts/m^2)')
Qave = mean(Power(StableRange))
Qprime = Qave/Area

```

Appendix A

MATLAB Programs

SimulatePlate.m

```
clc
clear all
close all

%% Import data from spreadsheet
clc
clear all
close all
wind = 1;
height = 12;
corr = 1;

%% Import the data
if height == 6;
    heightnum = 1;
    if wind == 0;
        [~, ~, raw] = xlsread('E:\YUMA\02_01_2016_SteelPlate_6in_sand_nofan.xlsx','02_01_2016_SteelPlate_6in_sand_', 'E2:H934');
        Change = 504;
        Qrad = 65.3696;
    else
        [~, ~, raw] = xlsread('E:\YUMA\02_02_2016_SteelPlate_6in_sand_fan.xlsx','02_02_2016_SteelPlate_6in_sand_', 'E2:H690');
        Change = 511;
    End

    windVect = ones(1,length(raw(:,1))).*1.2;
    Qrad = 67.5486;

elseif height == 12;
heightnum = 2;
    if wind == 0;
```

```

[~, ~, raw] =
xlsread('E:\YUMA\02_08_2016_SteelPlate_12in_sand_nofan.xlsx','02_08_2016_SteelPlate_
12in_sand','E2:H1201');
Change = 741;
else
[~, ~, raw] =
xlsread('E:\YUMA\02_05_2016_SteelPlate_12in_sand_fan.xlsx','02_05_2016_SteelPlate_12i
n_sand','E2:H734');
Change = 624;
end
windVect = ones(1,length(raw(:,1))).*1.8;
Qrad = 42.5917;

elseif height == 18;
heightnum = 3;

if wind ==0;
[~, ~, raw] =
xlsread('E:\YUMA\02_15_2016_SteelPlate_18in_sand_nofan.xlsx','02_15_2016_SteelPlate_
18in_sand','E2:H1732');
Change = 984;

else
[~, ~, raw] =
xlsread('E:\YUMA\02_12_2016_SteelPlate_18in_sand_fan.xlsx','02_12_2016_SteelPlate_18i
n_sand','E2:H833');
Change = 680;
End

windVect = ones(1,length(raw(:,1))).*1.3; %1.7
Qrad = 25.1861;

else error('Height not recorded')
end

%% Create output variable
data = reshape([raw{:}],size(raw));

%% Allocate imported array to column variable names
T1 = data(:,1);
T2 = data(:,2);
T3 = data(:,3);
T4 = data(:,4);

```

```

%% Clear temporary variables
clearvars data raw;

%% Constants
g = 9.807; %acceleration due to gravity (m/s^2)
A = 8*6*0.00064516; %Area of top surface (m^2)
P = (8+6)*2*0.0254; %Perimeter of top surface (m)
L = A/P; %Effective Length of Plate (m)
sigma = 5.670373*10^-8; %J/K^4*m^2*s
ep = .8;
dt = 30;
VolumeIn = .25*6*8; %in^3
Volume = VolumeIn*.0000163871;
Density = 7832; %Kg/m^3
Density2 = 7870; %Kg/m^3
Conductivity = 51.9; %W/mK
m2 = Volume*Density2;
n = 1.540124; %Kg
Area = 0.03096768; %m^2
Cp = 486*m2; %J/K
Qprime = Qrad/Area
absorp = .6; %Solar Absorbance

for n = 1:length(T1)
    time(n) = 30*(n-1);
end
%% Dividing temperature Data into categories
T1F = T1.*9/5+32;
T2F = T2.*9/5+32;
T3F = T3.*9/5+32;
T4F = T4.*9/5+32;
T1Heat = T1(1:Change);
T2Heat = T2(1:Change);
T3Heat = T3(1:Change);
T4Heat = T4(1:Change);
T1Cool = T1(Change+1:length(T1));
T2Cool = T2(Change+1:length(T2));
T3Cool = T3(Change+1:length(T3));
T4Cool = T4(Change+1:length(T4));
TAveCool = (T1Cool+T2Cool)./2;
timeheat = time(1:Change);
timecool = time(Change+1:length(T4));
TempDiff = T1-T4;
TempDiffHeat = TempDiff(1:Change);

```

```

TempDiffCool = TempDiff(Change:length(TempDiff));

%% Simulation
TSurfaceFull(1)= T1(1);
TSurfaceFullW(1)= T1(1);
TempChangeFull(1) = (T1(2)-T1(1))/(time(2)-time(1));

[~, ~, raw] = xlsread('E:\YUMA\HeatTransferProperties.xlsx','AirK','A2:H36');

%% Create output variable
data = reshape([raw{:}],size(raw));

%% Allocate imported array to column variable names
TAirData = data(:,1); %Temperature values of Air in C
rhoAirData = data(:,2); %Density values of air in kg/m^3
KAirData = data(:,4); % Thermal conductivity of air in W/mK
alphaAirData = data(:,5); %in m^2/s
DynViscAirData = data(:,6); %Dynamic viscosity of air in Ns/m^2
KinViscAirData = data(:,7); %Kinematic viscosity of air in m^2/s
PrAirData = data(:,8); %Prandtl Number of air

%% Clear temporary variables
clearvars data raw;

for n = 1:length(time)-1
    dt(n) = time(n+1)-time(n);
    Tf(n) = (T4(n)+TSurfaceFull(n))/2;
    TfW(n) = (T4(n)+TSurfaceFullW(n))/2;

xA(n) = find(TAirData>Tf(n), 1, 'first') ;
AirPercentage(n) = (Tf(n)-TAirData(xA(n)-1))/(TAirData(xA(n))-TAirData(xA(n)-1));
%Used to interpolate air values
rho(n) = AirPercentage(n)*(rhoAirData(xA(n))-rhoAirData(xA(n)-1))+rhoAirData(xA(n)-1);
%Finds density of air given the temperature
mu(n) = AirPercentage(n)*(DynViscAirData(xA(n))-DynViscAirData(xA(n)-1))+DynViscAirData(xA(n)-1); %Finds dynamic viscosity of air given the temperature
nu(n) = AirPercentage(n)*(KinViscAirData(xA(n))-KinViscAirData(xA(n)-1))+KinViscAirData(xA(n)-1); %Finds kinematic viscosity of air given the temperature
K(n) = AirPercentage(n)*(KAirData(xA(n))-KAirData(xA(n)-1))+KAirData(xA(n)-1);
%Finds conductivity of air given the temperature
alpha(n) = AirPercentage(n)*(alphaAirData(xA(n))-alphaAirData(xA(n)-1))+alphaAirData(xA(n)-1); %Finds alpha of air given the temperature
Pr(n) = AirPercentage(n)*(PrAirData(xA(n))-PrAirData(xA(n)-1))+PrAirData(xA(n)-1);
%Finds Prandtl number of air given the temperature

```

```

xAW(n) = find(TAirData>TfW(n), 1, 'first') ;
TfW(n) = (T4(n)+TSurfaceFullW(n))/2;
AirPercentageW(n) = (TfW(n)-TAirData(xAW(n)-1))/(TAirData(xAW(n))-TAirData(xAW(n)-1)); %Used to interpolate air values
rhoW(n) = AirPercentageW(n)*(rhoAirData(xAW(n))-rhoAirData(xAW(n)-1))+rhoAirData(xAW(n)-1); %Finds density of air given the temperature
muW(n) = AirPercentageW(n)*(DynViscAirData(xAW(n))-DynViscAirData(xAW(n)-1))+DynViscAirData(xAW(n)-1); %Finds dynamic viscosity of air given the temperature
nuW(n) = AirPercentageW(n)*(KinViscAirData(xAW(n))-KinViscAirData(xAW(n)-1))+KinViscAirData(xAW(n)-1); %Finds kinematic viscosity of air given the temperature
KW(n) = AirPercentageW(n)*(KAirData(xAW(n))-KAirData(xAW(n)-1))+KAirData(xAW(n)-1); %Finds conductivity of air given the temperature
alphaW(n) = AirPercentageW(n)*(alphaAirData(xAW(n))-alphaAirData(xAW(n)-1))+alphaAirData(xAW(n)-1); %Finds alpha of air given the temperature
PrW(n) = AirPercentageW(n)*(PrAirData(xAW(n))-PrAirData(xAW(n)-1))+PrAirData(xAW(n)-1); %Finds Prandtl number of air given the temperature

```

```

Beta(n) = 1/(Tf(n)+273);
DeltaT(n) = (TSurfaceFull(n)-T4(n));
Ra(n) = g*Beta(n)*abs(DeltaT(n))*L^3/(alpha(n)*nu(n));
Nu(n) = .54*Ra(n)^(1/4);
H(n) = K(n)*Nu(n)/L*A; %W/K or W/C
RadiationLoss(n) = ep*A*sigma*((T4(n)+273)^4-(TSurfaceFull(n)+273)^4);
QConv(n) = H(n)*(T4(n)-TSurfaceFull(n)); % Watts

```

```

if n < Change
Q(n) = Qrad*absorp;
else
Q(n) = 0;
End

```

```

TempChange(n+1) = (QConv(n)+RadiationLoss(n)+Q(n))/Cp;
TSurfaceFull(n+1) = TSurfaceFull(n) + (TempChange(n)+TempChange(n+1))*dt(n)/2;
BetaW(n) = 1/(TfW(n)+273);
DeltaTW(n) = (TSurfaceFullW(n)-T4(n));
RaW(n) = g*BetaW(n)*abs(DeltaTW(n))*(L)^3/(alphaW(n)*nuW(n));
ReW(n) = windVect(n)*(6*0.0254)/nuW(n); %6*0.0254
NuW(n) = .664*ReW(n)^(1/2)*PrW(n)^(1/3); %Forced Convection Laminar Flow
HW(n) = KW(n)*NuW(n)/L*A; %W/K or W/C
RadiationLossW(n) = ep*A*sigma*((T4(n)+273)^4-(TSurfaceFullW(n)+273)^4);
QConvW(n) = HW(n)*(T4(n)-TSurfaceFullW(n)); % Watts

```

```

if n < Change

```

```

    QW(n) = Qrad*absorp;
else
    QW(n) = 0;
end
TempChangeW(n+1) = (QConvW(n)+RadiationLossW(n)+QW(n))/Cp;
TSurfaceFullW(n+1) = TSurfaceFullW(n) +
(TempChangeW(n)+TempChangeW(n+1))*dt(n)/2;

end
figure (5)
timeplot = time/3600;

hold on

if wind == 0
plot(timeplot,TSurfaceFull,'k');
title(['Radiaton Simulaton for Height ',num2str(heightnum)])

else
plot(timeplot,TSurfaceFullW,'k');
title(['Radiaton Simulaton with Wind for Height ',num2str(heightnum)])
end

plot(timeplot,T1)
plot(timeplot,T4,':')
plot(timeplot,T3,'r--')

xlabel('Time (hours)')
ylabel(['Temperature ',char(176),'C'])
if wind == 0
legend('Simulation','Raw Data Top','Ambient Air', 'Sand Temperature')
else
legend('Wind Simulation','Raw Data Top','Ambient Air', 'Sand Temperature')
end

```

Appendix A

MATLAB Programs

YumaTripPlateAnalysis.m

```
clc
clear all
close all

%% Import the data
[~, ~, raw] = xlsread('E:\YUMA\Yuma Trip\8_19_2015_LoggerE.xlsx','8_19_2015_LoggerE','B2:D3106');
[~, ~, raw2] = xlsread('E:\YUMA\Yuma Trip\8_19_2015_LoggerE.xlsx','Weather','A2:D29');

%% Create output variable
data = reshape([raw{:}],size(raw));
data2 = reshape([raw2{:}],size(raw2));

%% Allocate imported array to column variable names
PlateTime = data(:,1);
T1Raw = data(:,2);
T2Raw = data(:,3);
WeatherTime = data2(:,1);
WeatherToD = data2(:,2);
TAmbRaw = data2(:,3);
Wind = data2(:,4);
absorp = .62; %Solar Absorbance

%% Clear temporary variables
clearvars data raw;

%% Time Vector
for n = 1:length(T1Raw)
    time(n) = 30*(n-1);
end

%%plot(WeatherTime, TAmbRaw, '*')
timeWFull = 0:.5:60;
TAmbFull = [];

for k=1:length(TAmbRaw)-1
    TAmbFullNew(k,:) = linspace(TAmbRaw(k),TAmbRaw(k+1),121);
    TAmbFull= [TAmbFull TAmbFullNew(k,1:length(TAmbFullNew)-1)];
end
```

```

end
AmbVect = TAmbFull(75:3179);

%% Constants
g = 9.81; %acceleration due to gravity (m/s^2)
A = 8*6*0.00064516; %Area of top surface (m^2)
P = (8+6)*2*0.0254; %Perimeter of top surface (m)
L = A/P; %Effective Length of Plate (m)
sigma = 5.670373*10^-8; %J/K^4*m^2*s
ep = .88;
dt = 30;
VolumeIn = .25*6*8; %in^3
Volume = VolumeIn*.0000163871;
Density = 7832; %Kg/m^3
Density2 = 7870; %Kg/m^3
m2 = Volume*Density2;
n = 1.540124; %Kg
Area = 0.03096768; %m^2
Cp = 486*m2; %J/K
T4C = smooth(smooth(5/9.*(AmbVect-32)));
T1C = smooth(smooth(5/9.*(T1Raw-32)));
T1CRaw = 5/9.*(T1Raw-32);
SunRange = 1:1500;
[~,~,raw] = xlsread('E:\YUMA\HeatTransferProperties.xlsx','Air','A2:H42');

%% Create output variable
data = reshape([raw{:}],size(raw));

%% Allocate imported array to column variable names
TAirData = data(:,1); %Temperature values of Air in C
KinViscAirData = data(:,7); %Kinematic viscosity of air in m^2/s
KAirData = data(:,4); % Thermal conductivity of air in W/mK
alphaAirData = data(:,5); %in m^2/s
PrAirData = data(:,8); %Prandtl Number of air

for i = SunRange

    dt(i) = time(i+1)-time(i);
    Tf(i) = (T4C(i)+T1C(i))/2;

    xA(i) = find(TAirData>Tf(i), 1,'first') ;
    AirPercentage(i) = (Tf(i)-TAirData(xA(i)-1))/(TAirData(xA(i))-TAirData(xA(i)-1)); %Used
    to interpolate air values

```

```

nu(i) = AirPercentage(i)*(KinViscAirData(xA(i))-KinViscAirData(xA(i)-1))+KinViscAirData(xA(i)-1); %Finds kinematic viscosity of air given the temperature
K(i) = AirPercentage(i)*(KAirData(xA(i))-KAirData(xA(i)-1))+KAirData(xA(i)-1); %Finds conductivity of air given the temperature
alpha(i) = AirPercentage(i)*(alphaAirData(xA(i))-alphaAirData(xA(i)-1))+alphaAirData(xA(i)-1); %Finds alpha of air given the temperature

```

```

Beta(i) = 1/(Tf(i)+273);
DeltaT(i) = (T1C(i)-T4C(i));
Ra(i) = g*Beta(i)*abs(DeltaT(i))*L^3/(alpha(i)*nu(i));
Nu(i) = .54*Ra(i)^(1/4);
H(i) = K(i)*Nu(i)/L*A; % W/K*m^2 or W/C
RadiationLoss(i) = ep*A*sigma*((T4C(i)+273)^4-(T1C(i)+273)^4);
QConv(i) = H(i)*(T4C(i)-T1C(i)); % Watts*m^2
Tdot(i) = (T1C(i+1)-T1C(i))/dt(i);
Power(i) = (Cp*Tdot(i)-RadiationLoss(i)-QConv(i))/absorp;

```

End

```

timeplot = time/3600;
Solar = Power./A;
f1 = polyfit(time(SunRange),Power(SunRange),5);
fitted = f1(1).*time.^5+f1(2).*time.^4+f1(3).*time.^3+f1(4).*time.^2+f1(5).*time+f1(6);
Qave = mean(Power(SunRange));
Sun = max(fitted)/A;
SunVect = fitted./A;
maxLocation = find(fitted./A==Sun);
scale = 1120/Sun;
f2 = f1.*scale;
plot(timeplot(SunRange),SunVect(SunRange),'k');
hold on
plot(timeplot(SunRange),Power(SunRange)/A);
xlabel('Time (Hours)')
ylabel('Watts/m^2')
legend('Polynomial Fit','Calculated Values')

```

%% Simulation

```

T1Sim(1) = T1C(1);
for i = SunRange
dt(i) = time(i+1)-time(i);
Tf(i) = (T4C(i)+T1Sim(i))/2;
xA(i) = find(TAirData>Tf(i), 1,'first') ;
AirPercentage(i) = (Tf(i)-TAirData(xA(i)-1))/(TAirData(xA(i))-TAirData(xA(i)-1)); %Used to interpolate air values

```

```

nu(i) = AirPercentage(i)*(KinViscAirData(xA(i))-KinViscAirData(xA(i)-1))+KinViscAirData(xA(i)-1); %Finds kinematic viscosity of air given the temperature
K(i) = AirPercentage(i)*(KAirData(xA(i))-KAirData(xA(i)-1))+KAirData(xA(i)-1); %Finds conductivity of air given the temperature
alpha(i) = AirPercentage(i)*(alphaAirData(xA(i))-alphaAirData(xA(i)-1))+alphaAirData(xA(i)-1); %Finds alpha of air given the temperature

Beta(i) = 1/(Tf(i)+273);
DeltaT(i) = (T1Sim(i)-T4C(i));
Ra(i) = g*Beta(i)*abs(DeltaT(i))*L^3/(alpha(i)*nu(i));
Nu(i) = .54*Ra(i)^(1/4);
H(i) = K(i)*Nu(i)/L*A; % W/K*m^2 or W/C
RadiationLoss(i) = ep*A*sigma*((T4C(i)+273)^4-(T1Sim(i)+273)^4);
QConv(i) = H(i)*(T4C(i)-T1Sim(i)); % Watts*m^2
Q(i) =
f2(1)*time(i)^5+f2(2)*time(i)^4+f2(3)*time(i)^3+f2(4)*time(i)^2+f2(5)*time(i)+f2(6);
if Q(i) < 0;
    Q(i) = 0;
end
TempChange(i+1) = (QConv(i)+RadiationLoss(i)+Q(i)*absorp)/Cp;
T1Sim(i+1) = T1Sim(i) + (TempChange(i)+TempChange(i+1))*dt(i)/2;
end

T1SimF = 9/5.*T1Sim+32;

figure
plot(timeplot(SunRange),T1Raw(SunRange));
hold on
plot(timeplot(SunRange),T1SimF(SunRange),'k');
legend('Data','Simulation')

T1SimWind(1) = T1C(1);

for i = 1:length(T1Raw)-1
    windVect(i) = .3;
    dtwind(i) = time(i+1)-time(i);
    Tfwind(i) = (T4C(i)+T1SimWind(i))/2;
    xAwind(i) = find(TAirData>Tfwind(i), 1,'first') ;
    AirPercentagewind(i) = (Tfwind(i)-TAirData(xAwind(i)-1))/(TAirData(xAwind(i))-TAirData(xAwind(i)-1)); %Used to interpolate air values
    nuwind(i) = AirPercentagewind(i)*(KinViscAirData(xAwind(i))-KinViscAirData(xAwind(i)-1))+KinViscAirData(xAwind(i)-1); %Finds kinematic viscosity of air given the temperature
    Kwind(i) = AirPercentagewind(i)*(KAirData(xAwind(i))-KAirData(xAwind(i)-1))+KAirData(xAwind(i)-1); %Finds conductivity of air given the temperature

```

```

alphawind(i) = AirPercentagewind(i)*(alphaAirData(xAwind(i))-alphaAirData(xAwind(i)-
1))+alphaAirData(xAwind(i)-1); % Finds alpha of air given the temperature
Prwind      =      AirPercentagewind(i)*(PrAirData(xAwind)-PrAirData(xAwind-
1))+PrAirData(xAwind-1); % Finds Prandtl number of air given the temperature
    Betawind(i) = 1/(Tf(i)+273);
    DeltaTwind(i) = (T1SimWind(i)-T4C(i));
    Rawind(i) = g*Betawind(i)*abs(DeltaTwind(i))*L^3/(alphawind(i)*nuwind(i));
    Re(i) = windVect(i)*6*0.0254/nuwind(i);
    Nuwind(i) = .664*Re(i)^(1/2)*Prwind(i)^(1/3); % Forced Convection Laminar Flow
    Hwind(i) = Kwind(i)*Nuwind(i)/L*A; % W/K*m^2 or W/C
    RadiationLosswind(i) = ep*A*sigma*((T4C(i)+273)^4-(T1SimWind(i)+273)^4);
    QConvwind(i) = Hwind(i)*(T4C(i)-T1SimWind(i)); % Watts*m^2
    Qwind(i) =
f2(1)*time(i)^5+f2(2)*time(i)^4+f2(3)*time(i)^3+f2(4)*time(i)^2+f2(5)*time(i)+f2(6);

if time(i) > 24*3600;
    Qwind(i) = f2(1)*(time(i)-24*3600/30)^5+f2(2)*(time(i)-24*3600/30)^4+f2(3)*(time(i)-
24*3600/30)^3+f2(4)*(time(i)-24*3600/30)^2+f2(5)*(time(i)-24*3600/30)+f2(6);
End

if Qwind(i) < 0;
    Qwind(i) = 0;
end

    TempChangewind(i+1) = (QConvwind(i)+RadiationLosswind(i)+Qwind(i)*absorp)/Cp;
    T1SimWind(i+1) =
(T1SimWind(i) +
(TempChangewind(i)+TempChangewind(i+1))*dtwind(i)/2;
end

max(Qwind)/A
figure
T1SimF2Wind = 9/5.*T1SimWind+32;
fullRange = 1:3104;
plot(timeplot(fullRange),T1CRaw(fullRange));
hold on
plot(timeplot(fullRange),T1SimWind(fullRange),'k');
plot(timeplot(fullRange),T4C(fullRange),':');
legend('Data','Simulation','Ambient')
xlabel('Time (Hours)')
ylabel('Temp (C)')

```

Appendix A

MATLAB Programs

MethodComparison.m

```
clc
clear all
close all

%% Import the data
[~, ~, raw] = xlsread('E:\YUMA\12_18_2014_NoCoating_6in.xlsx','12_18_2014_NoCoating_6in','E2:G721');
[~, ~, raw2] = xlsread('E:\YUMA\12_17_2014_InteriorCoating_6in.xlsx','12_17_2014_InteriorCoating_6in','E2:G721');
[~, ~, raw3] = xlsread('E:\YUMA\12_19_2014_Foil_6in_NoSleeve.xlsx','12_19_2014_Foil_6in_NoSleeve','C1:E722');
[~, ~, raw4] = xlsread('E:\YUMA\01_05_2015_Box_Sleeve_NoTape_6in.xlsx','01_05_2015_Box_Sleeve_NoTape_6i','C1:E531');
[~, ~, raw5] = xlsread('E:\YUMA\HoodTest6_2_2015.xlsx','HoodTest6_2_2015','F2:I161');
[~, ~, raw6] = xlsread('E:\YUMA\Data Summary From Trip.xlsx','Data Plate and Coat','C2:F3106');
[~, ~, raw7] = xlsread('E:\YUMA\Data Summary From Trip.xlsx','Data Day 2 No Hood SUV','C2:E311');
[~, ~, raw8] = xlsread('E:\YUMA\Data Summary From Trip.xlsx','Data Day 2 No Hood SUV','G2:I311');
[~, ~, raw9] = xlsread('E:\YUMA\Data Summary From Trip.xlsx','Data Day 1 Hood vs No Hood','C7:F233');
[~, ~, raw10] = xlsread('E:\YUMA\Data Summary From Trip.xlsx','Data Day 1 Hood vs No Hood','I7:K233');
[~, ~, raw11] = xlsread('E:\YUMA\Data Summary From Trip.xlsx','Data Coating vs. No Coating','I9:L109');
[~, ~, raw12] = xlsread('E:\YUMA\Data Summary From Trip.xlsx','Data Coating vs. No Coating','C9:E125');
[~, ~, raw13] = xlsread('E:\YUMA\Data Summary From Trip.xlsx','Data Day 2 Takachi SUV','C2:E63');
[~, ~, raw14] = xlsread('E:\YUMA\Data Summary From Trip.xlsx','Data Day 2 Takachi SUV','G2:I63');

%% Create output variable
```

```

data = reshape([raw{:}],size(raw));
data2 = reshape([raw2{:}],size(raw2));
data3 = reshape([raw3{:}],size(raw3));
data4 = reshape([raw4{:}],size(raw4));
data5 = reshape([raw5{:}],size(raw5));
data6 = reshape([raw6{:}],size(raw6));
data7 = reshape([raw7{:}],size(raw7));
data8 = reshape([raw8{:}],size(raw8));
data9 = reshape([raw9{:}],size(raw9));
data10 = reshape([raw10{:}],size(raw10));
data11 = reshape([raw11{:}],size(raw11));
data12 = reshape([raw12{:}],size(raw12));
data13 = reshape([raw13{:}],size(raw13));
data14 = reshape([raw14{:}],size(raw14));

```

```

%% Allocate imported array to column variable names
T1NoCoating = data(:,1);% *9/5+32; % Internal Box Temp
T2NoCoating = data(:,2);% *9/5+32; % External Box Temp
T3NoCoating = data(:,3);% *9/5+32; % Ambient Air Temp
T1Coating = data2(:,1);% *9/5+32; % Internal Box Temp
T2Coating = data2(:,2);% *9/5+32; % External Box Temp
T3Coating = data2(:,3);% *9/5+32; % Ambient Air Temp
T1Tape = data3(:,1);% *9/5+32; % Internal Box Temp
T2Tape = data3(:,2);% *9/5+32; % External Box Temp
T3Tape = data3(:,3);% *9/5+32; % Ambient Air Temp
T1Sleeve = data4(:,1);% *9/5+32; % Internal Box Temp
T2Sleeve = data4(:,2);% *9/5+32; % External Box Temp
T3Sleeve = data4(:,3);% *9/5+32; % Ambient Air Temp
T1Hood = 5/9*(data5(:,1)-32); % Top Surface of the Hood
T2Hood = 5/9*(data5(:,2)-32); % Bottom Surface of the Hood
T3Hood = 5/9*(data5(:,3)-32); % Under the Hood
T4Hood = 5/9*(data5(:,4)-32); % Ambient Temperature
diff = T3Hood-T4Hood;
maxDiff = max(diff)
PCStatic = 5/9*(data6(:,3)-32); % Powder Coated Box during static test
NCStatic = 5/9*(data6(:,4)-32); % Box with no powder coating during static test

timePCDynamic = data11(:,1)/3600; %Time for the powder coat dynamic test

PCDynamicBottom = 5/9*(data11(:,2)-32); %Temperature of the bottom interior of the powder
coated box during dynamic test
PCDynamicTop = 5/9*(data11(:,3)-32); %Temperature of the top interior of the powder coated
box during dynamic test

```

```

PCDynamicExt = 5/9*(data11(:,4)-32); %Temperature of the top exterior of the powder coated
box during dynamic test
NCDynamicBottom = 5/9*(data12(:,1)-32); %Temperature of the bottom interior of the plain
box during dynamic test
NCDynamicTop = 5/9*(data12(:,2)-32); %Temperature of the top interior of the plain box
during dynamic test
NCDynamicExt = 5/9*(data12(:,3)-32); %Temperature of the top exterior of the plain coated
box during dynamic test
Day1HoodBottom = 5/9*(data9(:,1)-32); %Temperature of the bottom interior of the box with
a hood Day 1
Day1HoodTop = 5/9*(data9(:,2)-32); %Temperature of the top interior of the box with a hood
Day 1
Day1HoodExt = 5/9*(data9(:,3)-32); %Temperature of the top exterior of the box with a hood
Day 1
Day1NoHoodBottom = 5/9*(data10(:,1)-32); %Temperature of the bottom interior of the box
without a hood Day 1
Day1NoHoodTop = 5/9*(data10(:,2)-32); %Temperature of the top interior of the box without
a hood Day 1
Day1NoHoodExt = 5/9*(data10(:,3)-32); %Temperature of the top exterior of the box without
a hood Day 1
Day2HoodBottom = 5/9*(data8(:,1)-32); %Temperature of the bottom interior of the box with
a hood Day 2
Day2HoodTop = 5/9*(data8(:,2)-32); %Temperature of the top interior of the box with a hood
Day 2
Day2HoodExt = 5/9*(data8(:,3)-32); %Temperature of the top exterior of the box with a hood
Day 2
Day2NoHoodBottom = 5/9*(data7(:,1)-32); %Temperature of the bottom interior of the box
without a hood Day 2
Day2NoHoodTop = 5/9*(data7(:,2)-32); %Temperature of the top interior of the box without a
hood Day 2
Day2NoHoodExt = 5/9*(data7(:,3)-32); %Temperature of the top exterior of the box without a
hood Day 2
Day2HoodBottomT = 5/9*(data14(:,1)-32); %Temperature of the bottom interior of the box
with a hood Day 2 for Takachi comparison
Day2HoodTopT = 5/9*(data14(:,2)-32); %Temperature of the top interior of the box with a
hood Day 2 for Takachi comparison
Day2TakachiBottom = 5/9*(data13(:,1)-32); %Temperature of the bottom interior of the
Takachi box Day 2
Day2TakachiTop = 5/9*(data13(:,2)-32); %Temperature of the top interior of the Takachi box
Day 2

%% Clear temporary variables
clearvars data data2 data3 data4 data5 data6 data7 data8 data9 data10 data11 data12 raw raw2
raw3 raw4 raw5 raw6 raw7 raw8 raw9 raw10 raw11 raw12;

```

```
%% Create Time Vectors
```

```
timeCoating = (0:30:30*(length(T1Coating)-1))./3600;  
timeNoCoating = (0:30:30*(length(T1NoCoating)-1))./3600;  
timeTape = (0:30:30*(length(T1Tape)-1))./3600;  
timeSleeve = (0:30:30*(length(T1Sleeve)-1))./3600;  
timeHood = (0:30:30*(length(T1Hood)-1))./3600;  
timePCStatic = (0:30:30*(length(PCStatic)-1))./3600;  
timeNCDynamic = (0:30:30*(length(NCDynamicTop)-1))./3600;  
timeDay1Hood = (0:30:30*(length(Day1HoodTop)-1))./3600;  
timeDay2Hood = (0:30:30*(length(Day2HoodTop)-1))./3600;  
timeDay2Takachi = (0:30:30*(length(Day2TakachiTop)-1))./3600;
```

```
%% Creating Plots
```

```
plot(timeCoating,T1Coating,'--k')  
hold on  
plot(timeCoating,T2Coating,'k')  
plot(timeCoating,T3Coating,':k')  
plot(timeNoCoating,T1NoCoating,'--')  
plot(timeNoCoating,T2NoCoating)  
plot(timeNoCoating,T3NoCoating,':')  
legend('Coating Internal','Coating External','Coating Ambient','Plain Internal','Plain External','Plain Ambient')  
title('Temperatures of Coating vs. No Coating')  
xlabel('Time (hours)')  
ylabel('Temperature in \circC')
```

```
figure
```

```
plot(timeTape,T1Tape,'--k')  
hold on  
plot(timeTape,T2Tape,'k')  
plot(timeTape,T3Tape,':k')  
plot(timeNoCoating,T1NoCoating,'--')  
plot(timeNoCoating,T2NoCoating)  
plot(timeNoCoating,T3NoCoating,':')  
legend('Tape Internal','Tape External','Tape Ambient','Plain Internal','Plain External','Plain Ambient')  
title('Temperatures of Tape vs. Plain')  
xlabel('Time (hours)')  
ylabel('Temperature in \circC')
```

```
figure
```

```
plot(timeSleeve,T1Sleeve,'--k')  
hold on
```

```

plot(timeSleeve,T2Sleeve,'k')
plot(timeSleeve,T3Sleeve,':k')
plot(timeNoCoating,T1NoCoating,'--')
plot(timeNoCoating,T2NoCoating)
plot(timeNoCoating,T3NoCoating,':')
legend('Air Pocket Internal','Air Pocket External','Air Pocket Ambient','Plain Internal','Plain External','Plain Ambient')
title('Temperatures of Sleeve vs. Plain')
xlabel('Time (hours)')
ylabel('Temperature in \circC')

```

```

figure
plot(timeHood,T1Hood,'k')
hold on
plot(timeHood,T2Hood,'--k')
plot(timeHood,T3Hood,':k')
plot(timeHood,T4Hood,':')
legend('Top of the Hood','Bottom of the Hood','Air Inside the Hood','Ambient')
title('Hood Test')
xlabel('Time (hours)')
ylabel('Temperature in \circC')

```

```

figure
plot(timePCStatic,PCStatic)
hold on
plot(timePCStatic,NCStatic,'k')
title('Static Powder Coat Test')
legend('Powder Coated','No Coat')
xlabel('Time (hours)')
ylabel('Temperature in \circC')

```

```

figure
plot(timePCDynamic,PCDynamicTop,'k')
hold on
plot(timePCDynamic,PCDynamicBottom,':k')
plot(timeNCDynamic,NCDynamicTop)
plot(timeNCDynamic,NCDynamicBottom,':')
title('Dynamic Powder Coat Test')
legend('Coated Top','Coated Bottom','Plain Top','Plain Bottom')
xlabel('Time (hours)')
ylabel('Temperature in \circC')

```

```

figure
hold on

```

```

plot(timeDay1Hood,Day1HoodTop,'k')
plot(timeDay1Hood,Day1HoodBottom,':k')
plot(timeDay1Hood,Day1NoHoodTop)
plot(timeDay1Hood,Day1NoHoodBottom,':')
title('Hood vs. No Hood Day 1')
legend('Box with Hood Top','Box with Hood Bottom','Box with No Hood Top','Box with No Hood Bottom')
xlabel('Time (hours)')
ylabel('Temperature in \circC')

```

```

figure
hold on
plot(timeDay2Hood,Day2HoodTop,'k')
plot(timeDay2Hood,Day2HoodBottom,':k')
plot(timeDay2Hood,Day2NoHoodTop)
plot(timeDay2Hood,Day2NoHoodBottom,':')
title('Hood vs. No Hood Day 2')
legend('Box with Hood Top','Box with Hood Bottom','Box with No Hood Top','Box with No Hood Bottom')
xlabel('Time (hours)')
ylabel('Temperature in \circC')

```

```

figure
hold on
plot(timeDay2Takachi,Day2HoodTopT,'k')
plot(timeDay2Takachi,Day2HoodBottomT,':k')
plot(timeDay2Takachi,Day2TakachiTop)
plot(timeDay2Takachi,Day2TakachiBottom,':')
title('Hood vs. Takachi')
legend('Box with Hood Top','Box with Hood Bottom','Takachi Box Top','Takachi Box Bottom')
xlabel('Time (hours)')
ylabel('Temperature in \circC')
axis([0 .52 42 54])

```

Appendix B

Air Property Tables

T (°C)	Density (Kg/m ³)	Specific Heat (J/Kg*K)	Thermal Conductivity (W/m*K)	Thermal Diffusivity (m ² /s)	Dynamic Viscosity (N*s/m ²)	Kinematic Viscosity (m ² /s)	Pr
-150	2.866	983	0.01171	4.16E-06	8.64E-06	3.01E-06	0.7246
-100	2.038	966	0.01582	8.04E-06	1.19E-05	5.84E-06	0.7263
-50	1.582	999	0.01979	1.25E-05	1.47E-05	9.32E-06	0.744
-40	1.514	1002	0.02057	1.36E-05	1.53E-05	1.01E-05	0.7436
-30	1.451	1004	0.02134	1.47E-05	1.58E-05	1.09E-05	0.7425
-20	1.394	1005	0.02211	1.58E-05	1.63E-05	1.17E-05	0.7408
-10	1.341	1006	0.02288	1.70E-05	1.68E-05	1.25E-05	0.7387
0	1.292	1006	0.02364	1.82E-05	1.73E-05	1.34E-05	0.7362
5	1.269	1006	0.02401	1.88E-05	1.75E-05	1.38E-05	0.735
10	1.246	1006	0.02439	1.94E-05	1.78E-05	1.43E-05	0.7336
15	1.225	1007	0.02476	2.01E-05	1.8E-05	1.47E-05	0.7323
20	1.204	1007	0.02514	2.07E-05	1.83E-05	1.52E-05	0.7309
25	1.184	1007	0.02551	2.14E-05	1.85E-05	1.56E-05	0.7296
30	1.164	1007	0.02588	2.21E-05	1.87E-05	1.61E-05	0.7282
35	1.145	1007	0.02625	2.28E-05	1.9E-05	1.66E-05	0.7268
40	1.127	1007	0.02662	2.35E-05	1.92E-05	1.7E-05	0.7255
45	1.109	1007	0.02699	2.42E-05	1.94E-05	1.75E-05	0.7241
50	1.092	1007	0.02735	2.49E-05	1.96E-05	1.8E-05	0.7228
60	1.059	1007	0.02808	2.63E-05	2.01E-05	1.9E-05	0.7202
70	1.028	1007	0.02881	2.78E-05	2.05E-05	2E-05	0.7177
80	0.9994	1008	0.02953	2.93E-05	2.1E-05	2.1E-05	0.7154
90	0.9718	1008	0.03024	3.09E-05	2.14E-05	2.2E-05	0.7132
100	0.9458	1009	0.03095	3.24E-05	2.18E-05	2.31E-05	0.7111
120	0.8977	1011	0.03235	3.57E-05	2.26E-05	2.52E-05	0.7073
140	0.8542	1013	0.03374	3.90E-05	2.35E-05	2.75E-05	0.7041
160	0.8148	1016	0.03511	4.24E-05	2.42E-05	2.98E-05	0.7014
180	0.7788	1019	0.03646	4.59E-05	2.5E-05	3.21E-05	0.6992
200	0.7459	1023	0.03779	4.95E-05	2.58E-05	3.46E-05	0.6974
250	0.6746	1033	0.04104	5.89E-05	2.76E-05	4.09E-05	0.6946
300	0.6158	1044	0.04418	6.87E-05	2.93E-05	4.77E-05	0.6935
350	0.5664	1056	0.04721	7.89E-05	3.1E-05	5.48E-05	0.6937

400	0.5243	1069	0.05015	8.95E-05	3.26E-05	6.22E-05	0.6948
450	0.488	1081	0.05298	1.00E-04	3.42E-05	7E-05	0.6965
500	0.4565	1093	0.05572	1.12E-04	3.56E-05	7.81E-05	0.6986
600	0.4042	1115	0.06093	1.35E-04	3.85E-05	9.52E-05	0.7037
700	0.3627	1135	0.06581	1.60E-04	4.11E-05	0.000113	0.7092
800	0.3289	1153	0.07037	1.86E-04	4.36E-05	0.000133	0.7149
900	0.3008	1169	0.07465	2.12E-04	0.000046	0.000153	0.7206
1000	0.2772	1184	0.07868	2.40E-04	4.83E-05	0.000174	0.726
1500	0.199	1234	0.09599	3.91E-04	5.82E-05	0.000292	0.7478
2000	0.1553	1264	0.11113	5.66E-04	6.63E-05	0.000427	0.7539